SP 130-4

Behavior of Ductile Multiple-Anchor Steel-to-Concrete Connections with Surface-Mounted Baseplates

by R. Cook and R. Klingner

Synopsis: A comprehensive research program has been conducted, dealing with ductile, multiple-anchor, steel-to-concrete connections. Based on the results of the program, behavioral models have been formulated for such connections, and design guidelines have been developed. In this paper, the program is summarized, and the principal results are reviewed.

Keywords: Anchors (fasteners); concretes; friction; loads (forces); shear properties; structural design; tension

Ronald A. Cook is an Assistant Professor of Civil Engineering at the University of Florida (Gainesville). Prior to holding that position, he was a Graduate Research Assistant at The University of Texas at Austin. He is a Member of ACI-ASCE Committee 355, Anchorage to Concrete.

Richard E. Klingner is the Phil M. Ferguson Professor of Civil Engineering at The University of Texas at Austin. Dr. Klingner is Chairman of ACI-ASCE Committee 442, Response of Concrete Buildings to Lateral Forces. He is a member of ACI-ASCE Committee 355, Anchorage to Concrete.

BACKGROUND AND INTRODUCTION

Design of multiple-anchor connections to concrete involves three steps:

1) calculation of the loads on the connection

2) distribution of those loads to the anchors

3) design of each anchor for its loads

This paper is concerned primarily with the second step. Existing information on the design of single ductile anchors, plus the experimental results of tests on multiple-anchor connections, are used to develop models for the behavior and design of multiple-anchor steel-to-concrete connections whose strength is controlled by the strength of the anchor steel. Complete results of this study are reported in Ref. 4, and have been incorporated into a Design Guide for Steel-to-Concrete Connections (5).

For the purposes of this study, all anchors were designed to be ductile according to the current provisions of ACI349 Appendix B (1). That is, all anchors were embedded sufficiently so that their pullout capacities, calculated using the 45° cone theory of ACI349 Appendix B, would exceed the fracture strength of the anchor steel. A ϕ factor of 0.65 was used, and the effects of edge distance and cone overlap were included where appropriate.

DEVELOPMENT OF EXPERIMENTAL PROGRAM

Objectives of Experimental Program

The behavior of a ductile multiple-anchor connection to concrete depends on a number of variables, including the following:

- loading (axial load, moment, shear)

- o size and configuration of steel attachment
- o size, number, location, and type of anchors
- o coefficient of friction between baseplate and concrete
- o tension/shear interaction for a single anchor
- o distribution of shear among anchors
- o distribution of tension among anchors
- o flexibility of baseplate

In a typical design situation only the loading is known. The designer must determine the size of the steel attachment and the size, number, location, and type of anchors. To complete this task, the designer must consider the effects of the last five variables. Present design standards (1,8,10) do not adequately address these variables. The purpose of the experimental program was to quantify and define these five variables for multiple-anchor connections to concrete.

The objectives of the experimental program were:

1) To determine the coefficient of friction between a surface-mounted steel baseplate and hardened concrete in multiple-anchor connections.

2) To determine tension/shear interaction relationships for cast-in-place anchors, undercut anchors, and adhesive anchors in multiple-anchor connections.

3) To determine the distribution of shear forces among anchors in multiple-anchor connections.

4) To determine the distribution of tension forces among anchors in multiple-anchor connections.

5) To determine the effect of baseplate flexibility on the behavior and design of multiple-anchor connections.

Since each of the variables being investigated could be studied in the absence of any externally applied axial load, the experimental program was limited to the study of multiple-anchor connections subjected to moment and shear only. This was accomplished by applying an eccentric shear load to several types of multiple-anchor connections at various load eccentricities.

The experimental program included the following types of tests:

1) Friction tests

2) Ultimate load tests:
   a) Two-anchor rigid baseplate tests
   b) Four-anchor rigid baseplate tests
   c) Six-anchor rigid baseplate tests
   d) Six-anchor flexible baseplate tests

Each type of test was developed to investigate one or more of the unknown variables.

Fig. 1 shows the basic loading condition used for all types of tests. In each test, measurements were made of the eccentric shear load, V, the eccentricity of the shear load, e, the individual anchor tension, T, the baseplate slip, δ_h, and the baseplate rotation, θ. For the ultimate load tests, connection failure was defined as the fracture of any anchor.

Development of Friction Tests

The purpose of the friction tests was to determine the coefficient of friction, μ, between a surface-mounted steel attachment and hardened concrete in a multiple-anchor connection. In this study, the coefficient of friction was evaluated by applying the compressive load to the attachment via tensile forces in the anchors, and then pulling on the attachment with an eccentric shear load until slip occurred. The tensile forces in the anchors were produced by anchor preload and/or by the forces developed to resist the external moment induced by the eccentric shear load. Oversized holes were provided to allow the plate to slip between the washers under the anchor nuts and the concrete as the eccentric shear load was applied.

In this test procedure, the total shear resistance comes from two frictional forces, shown in Fig. 2. One frictional force occurs between the washers and the baseplate, and is equal to the coefficient of friction between the washer and the baseplate, μ_s, multiplied by the total tensile force in all the anchors, ΣT. The other frictional force develops between the baseplate and the concrete, and is equal to the coefficient of friction between the baseplate and the concrete, μ, multiplied by the total compressive force across the steel/concrete interface.

Knowing the tension force in the anchors, ΣT, then the total compression force, C, across the steel/concrete interface is also known regardless of the eccentricity of the applied shear load. The condition of normal force equilibrium is given by:

$$C = \Sigma T \tag{1}$$

Since the applied shear, V, and the total anchor tension, ΣT, are measured as the steel attachment slips, the coefficient of friction between the baseplate and concrete, μ, is determined by the condition of shear force equilibrium as:

$$V = \mu C + \mu_s \Sigma T$$

Substituting Eq. (1) gives:

$$V = \mu \Sigma T + \mu_s \Sigma T$$

$$\mu = (V / \Sigma T) - \mu_s \qquad (2)$$

where: μ = coefficient of friction between the baseplate and the concrete

μ_s = coefficient of friction between the washers and the baseplate

The coefficient of friction between the baseplate and the concrete, μ, was determined by using a material with a known coefficient of friction between the washer and the baseplate, μ_s, in the friction tests.

The coefficient of friction between the baseplate and the concrete, μ, is applicable to connections where the anchors bear against the baseplate. In this situation the anchors displace with the baseplate and the only frictional force is between the baseplate and the concrete.

The anchors begin to bear on the baseplate when the applied shear load exceeds the effective frictional force of the connection. The ultimate load tests were all in this category. To analyze this type of connection the coefficient of friction for steel on concrete, μ, must be evaluated. Before all but two of the ultimate load tests, a friction test was conducted using the same specimen, so that a unique coefficient of friction could be determined for each ultimate load test.

Development of Ultimate Load Tests

Two-anchor rigid baseplate tests--The purpose of the two-anchor rigid baseplate tests was to determine the tension/shear interaction relationship for various types of anchors. Fig. 3 shows a free-body diagram of a typical two-anchor rigid baseplate specimen.

Using the coefficient of friction determined by the friction test, μ, the anchor tension, T_1, and applied shear, V, the amount carried by the anchors, V_1, is calculated as:

$$V_1 = V - (\mu T_1) \qquad (3)$$

where: $\mu T_1 \leq V$

By loading at different eccentricities, several combinations of anchor tension and anchor shear were recorded. The results were used to determine the tension/shear interaction relationship for the anchors.

Four-anchor rigid baseplate tests--The four-anchor rigid baseplate tests were developed to determine the distribution of shear among anchors. Fig. 4 shows a free-body diagram of a typical four-anchor rigid baseplate specimen. The difference between the two-anchor tests and the four-anchor tests is the contribution of the shear strength of the anchors on the compression end of the steel attachment.

Individual anchor shear was not measured. By using the coefficient of friction from the friction test, the tension/shear interaction relationship developed from the two-anchor tests, and the measured values of anchor tension, the amount of shear redistribution in the connection at failure can be evaluated. For example: If the total applied shear load at failure is equal to the sum of the frictional force between the concrete and the steel, plus the pure shear strength of the anchors on the compression end of the connection, plus the residual shear strength of the tension-end anchors based on their tension/shear interaction, then full redistribution of shear has occurred in the connection.

Six-anchor rigid baseplate tests--The six-anchor rigid baseplate tests were developed to determine the distribution of tension among the anchors, and to verify if the method of shear distribution determined from the four-anchor tests could be extended to a six-anchor configuration. Fig. 5 shows a free body diagram of a typical six-anchor rigid baseplate specimen.

The difference between the six-anchor tests and the four-anchor tests was the addition of a middle row of anchors. From a design viewpoint this is a very inefficient location for additional anchors. For additional moment capacity the anchors should be placed toward the tension end of the connection; for additional shear capacity the anchors should be placed toward the compression end of the connection, so that their shear capacity is not diminished by tensile forces. Because the purpose of these tests was to determine the distribution of tension and shear in an extreme situation, the anchors were placed at the centerline of the connection. Since the anchor tension was measured for all anchors, the distribution of tensile forces in the connection was known throughout the test.

Six-anchor flexible baseplate tests--The primary purpose of the six-anchor flexible baseplate tests was to evaluate the effects of baseplate flexibility on the location of the compressive resultant. A secondary purpose was to determine if the methods of predicting shear and tension distribution developed in the rigid baseplate tests could be extended to connections with flexible baseplates.

In a rigid baseplate test there is no flexibility in the steel attachment, and the compressive reaction from applied moment is located at the leading edge of the plate. In a flexible baseplate

loaded with applied moment, the portion of the baseplate extending beyond the attached member bends and causes the compressive reaction to shift inward from the leading edge. Fig. 6 shows a free-body diagram of a typical six-anchor flexible baseplate specimen. Since the applied moment, (V x e), and the anchor tensions, T_1 and T_2, were measured, the internal moment arm for the outer row of tension anchors, d_1, is calculated by the condition of moment equilibrium as:

$$V\ e = T_1\ d_1 + T_2\ (\ d_1 - s\ )$$

$$d_1 = (\ V\ e - T_2\ s\ )\ /\ (\ T_1 + T_2\ ) \qquad (4)$$

The location of the compressive reaction, as determined by Eq. (4), can be compared to what would be predicted by various procedures, described in more detail in Subsection 2.3.1 of Ref. 4. The appropriate method of analysis for determining the internal moment arm and the location of the compressive resultant for flexible baseplates can then be determined.

Choice of anchor pattern--The anchor pattern chosen for the experimental study was consistent with what is required to develop the plastic moment capacity of a W12 steel beam with a yield strength of 36 ksi using 5/8-inch diameter ASTM A193-B7 anchors. This beam size, while selected arbitrarily, is typical of that used in such connections.

The maximum design moment capacity of the six-anchor rigid baseplate (Fig. 5), as limited by the strength of the anchor steel, was determined using the following assumptions:

1) The compressive reaction from the applied moment was assumed to be at the toe of the plate.

2) The tensile forces, T_3, in the anchors on the compression end of the plate were assumed to be zero.

3) The tensile forces in the extreme tension anchors, T_1, and the middle row of anchors, T_2, were assumed to be at their design tensile strength.

4) The design tensile strength of the anchors was determined using the procedures of the AISC LRFD Specification as given in Table 1.

The calculated maximum design moment capacity of the connection, as limited by the strength of the anchor steel, was sufficient to develop the plastic moment capacity of a W12x22 steel beam:

$$\phi\ M = \phi\ T_1\ d_1 + \phi\ T_2\ d_2$$

$$\phi M = \phi A_s F_u (d_1 + d_2)$$

$$\phi M = (0.75) [(2) (0.226)] (125) (17 + 9)$$

$$\phi M = 1102 \text{ in-k} = 91.8 \text{ k-ft}$$

Embedment design basis--The embedded length of the anchors was determined using the provisions of ACI 349-85 (1) for cast-in-place and undercut anchors, and using the results of the study by Collins et al (3) for adhesive anchors. For the cast-in-place and undercut anchors, the required embedded length necessary to develop the six-anchor pattern was determined to be 11 inches by the procedures of ACI 349-85.

The required embedded length for adhesive anchors was determined by applying a capacity reduction factor, ϕ, of 0.65 to the embedded length which typically failed the steel for single 5/8-inch diameter ASTM A193-B7 adhesive anchors in the tests reported by Collins et al (3). The corresponding required embedded length was determined to be 11 inches. Therefore, an 11-inch embedded length was used for all types of anchors in all types of tests.

Rigid baseplate design basis--Although the anchor patterns were developed to be consistent with connecting a W12 steel beam, it was not possible, using a W12 member, to obtain rigid baseplate behavior, and also provide an adequate interface with the test frame. To provide a steel attachment that would rotate as a rigid body, the attached member was constructed of two 1-inch plates separated by 3-1/4 inches, extending the full length of the baseplate, and welded to the baseplate with full-penetration welds. The plate separation was required for attaching the horizontal loading arm of the test frame. Fig. 7 shows the steel attachment used for the rigid baseplate tests. The eccentricities shown in Fig. 7 were intended to produce a range of anchorage behavior.

The overall thickness of the baseplate was 2 inches, sufficient to prevent yielding of the baseplate near the attached member. The baseplate was counterbored 1/2 inch deep by 2-1/4 inches diameter around the anchor hole centerlines, reducing the baseplate thickness to 1-1/2 inches at the anchors. This provided a reasonable projected anchor length above the surface of the concrete.

The anchor holes were 7/8 inches in diameter. This corresponded to a 1/4-inch oversize hole for the 5/8-inch diameter anchors, which is larger than the 3/16-inch oversize permitted by the AISC LRFD Specification (9). The large oversize was to accommodate construction tolerances and to provide a probable worst case for redistribution of shear in the connection.

Flexible baseplate design basis--The flexible baseplate was designed to yield on the compression end of the baseplate, and be at or just above yield on the tension end of the baseplate at anchor failure. The particular design chosen was meant to represent a reasonable limit on plate flexibility. If the plate were more flexible (thinner), a plastic hinge would form on the tension end of the baseplate, possibly causing prying forces in the anchors.

The six-anchor flexible baseplate dimensions were chosen based on using a 12-inch deep member on a 20-inch deep baseplate with the same anchor pattern as the rigid baseplate tests. The flexible baseplate was 2 inches longer than the rigid baseplate. The extra 2 inches in length was provided to increase the flexibility of the baseplate. The attached member was constructed using two 12-inch channel sections separated by 5-1/4 inches. The channel separation was required for two 1-inch plates and the horizontal loading arm of the test frame. Fig. 8 shows the steel attachment used for the flexible baseplate tests. The eccentricity shown in Fig. 8 was selected to ensure that all anchors would contribute in shear. This is discussed later in the section dealing with the behavioral model.

The plate thickness was determined by assuming that at ultimate a force equal to the yield strength of the outer row of tension anchors would be applied to the baseplate at the tension anchor holes. The baseplate, acting as a tip-loaded cantilever, would have to be thick enough to avoid the formation of a plastic hinge at the edge of the tension flange of the attached member. The effective width of the cantilever was taken as the plate width, b. The design flexural strength of the baseplate, ϕM_p, was determined using the provisions of the AISC LRFD Specification (9). Fig. 9 shows the design basis for determining the thickness of the flexible baseplate. The flexible baseplate thickness was determined as:

$$\phi M_p \geq 2 A_s F_y d'$$

$$\phi F_y \left(b t^2 / 4 \right) \geq 2 A_s F_y d'$$

$$0.9 (36) \left(12 t^2 / 4 \right) \geq 2 (0.226) (105) (2)$$

$$t \geq 1 \text{ inch}$$

Since the actual tensile forces in the anchors were expected to exceed the yield strength of the anchors it was considered likely that yielding would occur on the tension end of the plate for the 1-inch plate thickness. If prying forces did not develop for this case, then baseplate thicknesses determined using the method described in Subsection 2.4.1 of Ref. 4 (based on the average tensile strength of the anchors rather than the yield strength), could be considered sufficient to prevent significant prying forces.

Since the compressive resultant in the six-anchor test would be equal to the load in the four tension anchors, the 4-inch portion of the plate projecting past the compression flange was expected to yield. This compression-end yielding was not expected to degrade

the performance of the attachment. As verified in the test program, this was in fact the case.

Description of Test Setup

The test setup, shown in Fig. 10, consisted of a test block, tied to the laboratory floor, and containing a steel attachment, connected to the test block by the anchors to be tested. The attachment was connected to the loading ram by a mechanical linkage consisting of a horizontal loading arm, a vertical loading beam, and an inclined hydraulic ram, operated under displacement control.

Test Instrumentation

Loads--The eccentric shear load, V, was measured by a commercially manufactured load cell installed in the horizontal loading arm. Individual anchor tensions were measured by specially constructed anchor load cells and adapters, which allowed the anchors to deform as in a connection without the anchor load cells.

Displacement and rotation--Slip relative to the surface of the concrete was measured using a linear potentiometer as shown in Fig. 11. For the rigid-baseplate case, the baseplate rotation, θ, was evaluated by measuring a single displacement, as shown in Fig. 12. The plate rotation, θ, could be evaluated as: $\theta = \delta_v / L$.

For the flexible baseplate, the baseplate rotation, θ, was not measured directly. Instead, the vertical displacement along the centerline of the baseplate was measured at several locations, as shown in Fig. 13.

Data acquisition and reduction--The loads and displacements for all tests were recorded using a Hewlett-Packard data acquisition system, and then converted to engineering units and stored using a program developed at the Ferguson Structural Engineering Laboratory and an IBM PC-AT compatible microcomputer. Data recorded by this system was obtained within 1 second after each displacement increment was imposed on the attachment. This data acquisition system is referred to here as "HP DAS."

Test Matrix and Test Designations

The test matrix is shown in Table 2. Three types of anchors were tested: cast-in-place (CIP); undercut (M1); and adhesive (A1-A6). Six different adhesives were included in the testing program: three epoxies (A1, A5, A6); two polyesters (A3, A4); and one

vinylester (A2). The specific brand names of the undercut and adhesive anchors are shown in Table 2. The test matrix was developed to assess the behavior of all types of anchors, over a wide range of shear load eccentricities.

One epoxy adhesive and one polyester adhesive were tested for all the anchor patterns. To permit comparison of results for the six adhesives, the other four adhesives were tested only in the six-anchor pattern at a 12-inch eccentricity, using the rigid baseplate.

Each rigid baseplate test was designated by the number of anchors in the pattern, the type of anchor, and the eccentricity of the applied shear load. For example: Test 6 CIP 12 refers to a six-anchor rigid baseplate test with cast-in-place anchors, loaded at a 12-inch eccentricity. Test 4 A4 6 refers to a four-anchor rigid baseplate test with type A4 adhesive anchors, loaded at a 6-inch eccentricity.

The test number for a flexible baseplate test is followed by an "x." For example: Test 6 M1 12x refers to a six-anchor flexible baseplate test with undercut anchors, loaded at a 12-inch eccentricity.

Materials

Concrete--The experimental program used a ready-mix concrete designed to meet Texas SDHPT Specifications for Class C concrete. The compressive strengths of 6- x 12-inch cylinders are shown in Table 3. Since the three test blocks from each concrete pour were tested on different dates, the compressive strength at the time of testing is shown as a range in Table 3. The concrete surface where the attachment was to be placed was screeded and then troweled once.

Anchors--Adhesive anchors and undercut anchors were 5/8-inch diameter ASTM A193-B7 threaded rod. Cast-in-place anchors were fabricated from 5/8-inch diameter ASTM A193-B7 plain rod, threaded on each end. The average tensile strength of the ten anchors was 31.2 kips, within 1% of the value determined from previous studies (3,6). As indicated by Table 4, there was no appreciable difference in tensile strength among the three types of anchors. The average tensile strength for all types of anchors was taken as 31.0 kips. All anchors were installed according to manufacturers' instructions, using a template to position the holes.

TEST RESULTS

Friction Tests

The results of the 44 friction tests performed in this study are shown in Table 5. That table also shows the test variables that were considered to have a possible effect on the coefficient of friction. These variables are the sequential number of the friction tests with the rigid baseplate, the test block surface, the magnitude of the compressive force, and the type of friction test. The effects of these variables are discussed later here.

In all types of friction tests, application of the eccentric shear load forced the centroid of the compressive force toward the leading edge, or toe, of the baseplate. This was especially true for friction tests, in which the compressive force was intentionally concentrated toward the leading edge prior to applying the shear load, so that the distribution of frictional force over the baseplate would correspond to that present in a baseplate under eccentric shear load.

Ultimate Load Tests

All ultimate-load specimens failed by yielding and fracture of the anchors. The strength of the connection was limited by the strength of the steel in all tests. Table 6 shows the maximum values of the applied shear load recorded by the HP Plotter and the HP DAS for those tests in which both data acquisition systems were used.

Load-displacement diagrams are presented in this section and in Appendix C of Ref. 4. Their principal purpose is to show the ductile behavior of connections dominated by anchor shear and also by anchor tension. The diagrams show the total displacement at the location of the outer row of tension anchors. The total displacement was determined as the square root of the sum of the squares of the horizontal slip, δ_h, and the vertical displacement, δ_v, at the location of the outer row of tension anchors.

The ultimate load tests showed that all types of anchors tested--cast-in-place, adhesive, and undercut--underwent significant inelastic shearing deformation before failure. They also showed that anchors transfer shear primarily by bearing. A shear-friction mechanism, which requires that a spalled wedge of concrete be confined by the baseplate, was not observed.

Two-anchor rigid baseplate tests-- Fig. 14 shows a typical load-displacement diagram for a two-anchor rigid baseplate test in which failure was dominated by anchor shear. Fig. 15 shows a

typical load-displacement diagram for a two-anchor rigid baseplate test in which failure was dominated by anchor tension. Load-displacement diagrams for other two-anchor rigid baseplate tests are shown in Appendix C of Ref. 4.

Four-anchor rigid baseplate tests--Fig. 16 shows a typical Load-displacement diagram for a four-anchor rigid baseplate test in which failure was dominated by anchor shear. Fig. 17 shows a typical load-displacement diagram for a four-anchor rigid baseplate test in which failure was dominated by anchor tension. Load-displacement diagrams for other four-anchor rigid baseplate tests are shown in Appendix C of Ref. 4.

Six-anchor rigid baseplate tests--Fig. 18 shows a typical load-displacement diagram for a six-anchor rigid baseplate test in which failure was dominated by anchor shear. Fig. 19 shows a typical load-displacement diagram for a six-anchor rigid baseplate test in which failure was dominated by anchor tension. Load-displacement diagrams for other six-anchor rigid baseplate tests are shown in Appendix C of Ref. 4.

Six-anchor flexible baseplate tests--Fig. 20 shows a typical load-displacement diagram for a six-anchor flexible baseplate test. Load-displacement diagrams for other six-anchor flexible baseplate tests are shown in Appendix C. Fig. 21 shows the vertical displacements along the centerline of the baseplate for a typical flexible baseplate test. As shown by that figure, the flexible baseplates rotated about a point very near the compression flange of the attached member (the compression flange was 4 inches from the leading edge). The actual contact zone between the baseplate and the concrete was found to be dependent on surface irregularities in the concrete finish.

DISCUSSION OF TEST RESULTS

Coefficient of Friction

The frequency distribution of the mean coefficient of friction for the friction tests is shown in Fig. 22. As indicated in Table 5, the average mean value is 0.43 with a standard deviation of 0.09. These results are in close agreement with the results of 15 previous friction tests (2,7), which showed an average value of 0.41 for the coefficient of friction for a surface-mounted steel plate installed on hardened concrete. The coefficient of friction was not significantly affected by the surface condition of the concrete, the magnitude of the compressive force, nor "digging in" of the toe of the rigid baseplate into the concrete. For design purposes, the

coefficient of friction, μ, should be taken as 0.40 with a strength reduction factor, ϕ, of 0.65.

Tension/Shear Interaction Relationships

The purpose of the two-anchor rigid baseplate tests was to determine the tension/shear interaction relationship for various types of anchors in a multiple-anchor connection. Results of the two-anchor rigid baseplate tests were used to construct tension/shear interaction diagrams for the three types of anchors studied in the experimental program. The anchor tensile forces were measured directly. The anchor shear forces presented in this subsection were calculated as discussed on page 6.

As shown by Figs. 23-25, an elliptical tension/shear interaction relationship provides a reasonable and generally conservative fit to the test data. A linear tension/shear interaction relationship is conservative.

Those same figures show that the shear strength (steel failure) of cast-in-place and adhesive anchors are the same. The shear strength of these anchors in a multiple-anchor connection should be taken as 50% of the tensile strength ($V_0/T_0 = \gamma = 0.50$). The shear strength (steel failure) of undercut anchors in a multiple-anchor connection should be taken as 60% of the tensile strength ($V_0/T_0 = \gamma = 0.60$).

Distribution of Tension and Shear among Anchors

Results of the four-anchor and six-anchor ultimate load tests indicated the following:

1) Tension and shear forces in the anchors redistribute inelastically as required to maintain equilibrium with the applied loading.

2) For connections dominated by moment (high eccentricity of the applied load) the anchors away from the toe of the baseplate attain their full tensile strength.

3) For connections dominated by shear (low eccentricity of the applied load) the ultimate strength of the connection is not sensitive to the distribution of tension in the anchors.

4) The initial distribution of anchor tension (prior to inelastic redistribution) has no effect on the ultimate strength of the connection.

Based on these observations, a limit design approach appears to be appropriate for ductile multiple-anchor connections. Limit

design requires that forces redistribute prior to failure and that the distribution of forces prior to redistribution not effect the ultimate strength. The following major section ("Theoretical Strength of Ductile Multiple-Anchor Connections") presents and assesses a behavioral model, based on limit design theory, for multiple-anchor connections to concrete.

Effect of Baseplate Flexibility

The effect of baseplate flexibility on the location of the compressive reaction can be determined by considering the concrete to be a rigid bearing surface, and the portions of the baseplate projecting beyond the compression flange of the attached member to be flexible. The portion of the baseplate welded to the attached member should be considered to rotate as a rigid body. The behavior of a flexible baseplate can be described as follows:

1) Initially, the baseplate rotates as a rigid body pivoting about the toe of the plate.

2) As the compressive load increases, the portion of the baseplate adjacent to the compressive element of the attached member reaches the yield moment, M_y, of the baseplate. This causes the compressive reaction, C, to move inward toward the compression element. This inward movement, shown in Fig. 26, is required to prevent the formation of a hinge at the edge of the compression element of the attached member. If a hinge forms, the overhanging projection of the baseplate becomes a mechanism.

3) Eventually, the compressive reaction moves as close to the compression element of the attached member as it can without exceeding the yield moment, M_y, of the plate adjacent to the compression element. The smallest distance, x_{min}, between the compressive reaction and the compression element of the attached member can be determined by:

$$x_{min} = M_y / C \qquad (5)$$

4) With a further increase in the compressive reaction, the baseplate begins to form a plastic hinge, M_p, and the compressive reaction, C, moves away from the compression element. The furthest distance that the compressive reaction moves away from the support is determined by:

$$x_p = M_p / C \qquad (6)$$

5) At this point, the overhanging projection of the baseplate becomes a mechanism. With a further increase in the magnitude of the compressive reaction, the location of the reaction will again approach the compression element of the attached member.

To locate the compressive reaction in a conservative manner, the reaction can be considered to be at a distance, x_{min}, determined by Eq. (5) from the edge of the compression element of the attached member.

THEORETICAL STRENGTH OF DUCTILE MULTIPLE-ANCHOR CONNECTIONS

Introduction to Theoretical Model

Fig. 27 shows the forces on a typical multiple-anchor connection. The anchors are assumed to have no preload, for two reasons: First, the assumption of no preload is conservative for calculation of frictional forces; and second, preload is irrelevant after the anchor has yielded, and this model is intended for use in a strength design of connections. The connection shown in Fig. 27 has one row of anchors in the compression zone and two rows of anchors in the tension zone. The behavior of a ductile multiple-anchor connection can be separated into three distinct ranges:

1) If the shear strength provided by the frictional force (developed from the compressive reaction produced by the applied moment) is larger than the applied shear, then anchors are not required for shear. The anchors in the tension zone can be assumed to develop their full tensile strength for moment resistance.

2) If the shear strength provided by the frictional force and by the anchors in the compression zone exceeds the applied shear, the anchors in the tension zone can be assumed to develop their full tensile strength for moment resistance.

3) If the shear strength provided by the frictional force and by the anchors in the compression zone is less than the applied shear, the anchors in the tension zone must transfer the remaining shear load. The strength of the anchors in the tension zone is limited by their tension/shear interaction.

The transitions between these three ranges of behavior can be determined by considering two critical values of shear load eccentricity, e. The shear load eccentricity, e, is equal to the moment to shear ratio, (M/V), of the applied loading at the surface of the concrete.

The first critical eccentricity, e', corresponds to the point at which the applied shear load is equal to the frictional force. For eccentricities larger than e', the connection does not slip and no shear anchors are required. For eccentricities smaller than e', the connection slips and shear anchors must be provided. The first critical eccentricity, e', represents the transition between Range 1 behavior and Range 2 behavior as described above.

The second critical eccentricity, e", corresponds to the point at which the applied shear load is equal to the sum of the frictional force and the shear strength of the anchors in the compression zone. For eccentricities larger than e", the anchors in the tension zone can be assumed to develop their full tensile strength for moment resistance. For eccentricities smaller than e", the anchors in the tension zone carry both tension and shear. The second critical eccentricity, e", represents the transition between Range 2 behavior and Range 3 behavior as described above.

The three ranges of behavior are shown in Fig. 28. Note that if no anchors are provided in the compression zone, Range 2 behavior is not applicable, and e" is the same as e'.

The strength of a ductile multiple-anchor connection can be summarized by considering two distinct areas of connection strength:

1) Strength Dominated by Moment: For $e \geq e''$, the strength of the connection is controlled by the tensile strength of the anchors in the tension zone. The connection has identical strength in Ranges 1 and 2. For connections without anchors in the compression zone, Range 2 does not exist, and the strength is dominated by moment when $e \geq e'$.

2) Strength Dominated by Shear: For $e < e''$, the strength of the connection is controlled by the shear strength of the anchors in the compression zone and the combined tensile and shear strength of the anchors in the tension zone. For connections without anchors in the compression zone, Range 2 does not exist, and the strength is dominated by shear when $e < e'$.

Analytical Development of the Behavioral Model

The strength of connections dominated by shear is dependent on the tension/shear interaction of the anchors. As noted previously, an elliptical interaction curve best describes the strength of a single anchor in combined tension and shear. A linear interaction is more conservative. An elliptical tension/shear interaction is used in the analytical development presented in this section. Since an elliptical interaction is difficult to apply in practice the corresponding linear formulations are also presented. The elliptical and linear tension/shear interactions are as given below:

1) For elliptical tension/shear interaction, the anchor shear strength is given by:

$$V_n = \gamma \sqrt{(T_0^2 - T_n^2)} \qquad (7)$$

2) For the more conservative linear tension/shear interaction, the anchor shear strength is given by:

$$V_n = \gamma (T_o - T_n) \quad (8)$$

where:

V_n = shear strength of an anchor in combined tension and shear

γ = ratio of the shear strength of the anchor to the tensile strength of the anchor

T_o = tensile strength of the anchor

T_n = tensile force in the anchor

The critical eccentricities, e' and e", can be determined by the conditions of equilibrium. Fig. 29 shows the forces on a typical multiple-anchor connection with a shear load eccentricity equal to e'. Fig. 30 shows the forces on a typical multiple-anchor connection with the shear load eccentricity equal to e".

The following formulations for the critical eccentricities, e' and e", are applicable to connections with multiple rows of anchors if "d" is taken as the distance from the compressive reaction, C, to the centroid of the anchors in the tension zone, "n" is taken as the number of rows of anchors in the tension zone, "m" is taken as the number of rows of anchors in the compression zone, and "T_0" is taken as the tensile strength of a row of anchors.

The minimum eccentricity, e', for multiple-anchor connections without shear anchors can be determined by the conditions of equilibrium when the applied shear load, V, is equal to the frictional force, μ C, (Fig. 29). The condition of shear force equilibrium for the connection shown in Fig. 29 is given by:

$$V = \mu C \quad (9)$$

The condition of normal force equilibrium for the connection shown in Fig. 29 is given by:

$$C = n T_0 \quad (10)$$

Substituting Eq. (9) into Eq. (10) yields the following:

$$V = \mu n T_0 \quad (11)$$

The moment equilibrium condition for the connection shown in Fig. 29 is given by:

$$V e' = n T_0 d$$

$$V = n T_0 d / e' \quad (12)$$

$$e' = d / \mu \quad (13)$$

where:

- e' = minimum eccentricity for multiple-anchor connections without shear anchors
- μ = coefficient of friction between steel and concrete
- d = distance from the compressive reaction to the centroid of the anchors in the tension zone

The minimum eccentricity, e", for multiple-anchor connections without combined tension and shear in the anchors can be determined by the conditions of equilibrium when the applied shear load, V, is equal to the sum of the frictional force, μ C, and the shear strength of the rows of anchors in the compression zone, m γ T_0. Fig. 30 only shows one row of anchors in the compression zone, (m = 1). The condition of shear force equilibrium for the connection shown in Fig. 30 is given by:

$$V = \mu C + m \gamma T_0 \quad (14)$$

Since the equation for normal force equilibrium is not changed by this formulation, Eq. (10) can be substituted into Eq. (14):

$$V = T_0 (n \mu + m \gamma) \quad (15)$$

Since the equation for moment equilibrium, Eq. (12), is not changed by this formulation (e" is substituted for e'), Eq. (15) can be set equal to Eq. (12) and the eccentricity, e", can be determined as:

$$e" = n d / (n \mu + m \gamma) \quad (16)$$

where:

- $e"$ = minimum eccentricity for multiple-anchor connections without combined tension and shear in the anchors
- n = number of rows of anchors in the tension zone
- m = number of rows of anchors in the compression zone
- μ = coefficient of friction between steel and concrete

γ = ratio of the shear strength of the anchor to the tensile strength of the anchor

d = distance from the compressive reaction to the centroid of the tension anchors

Note that e" reduces to e' when no anchors are provided in the compression zone.

Distribution of tension--As noted in the previous section, for connections with more than one row of anchors in the tension zone the distribution of tension cannot be adequately predicted by traditional design methods. In limit design theory, the assumed distribution of tensile forces has no effect on the actual strength of the connection. As long as sufficient anchors are provided to satisfy the conditions of equilibrium, the connection will perform satisfactorily.

In applying limit design theory, the issue of available inelastic deformation capacity must be addressed. Limit design theory is based on the assumption that materials have infinite plastic deformation capacity after yield. This is not the case. In a connection with two or more rows of anchors, subjected to an applied moment (Fig. 31), if the inner row of tension anchors is too close to the compressive reaction, anchors there will not be able to reach their tensile strength before the available deformation capacity is exceeded in the outer row of tension anchors.

Anchor materials typically have a specified minimum elongation requirement of at least 10% in 2 inches. This represents an ultimate strain, ϵ_u, of 0.10 or greater. To ensure that the tensile force in the inner row of anchors reaches the minimum specified tensile strength of the anchors, the distance between the inner row of anchors and the compressive reaction, d_2, should not be less than about 10% of the distance from the outer row of anchors to the compressive reaction, d_1 ($d_2 \geq 0.10\ d_1$ in Fig. 31). The reason for this is as follows. When the inner row of anchors is so located, the tensile strain there, ϵ_2, will be at least 0.01 when the tensile strain in the outer row of anchors, ϵ_1, reaches its maximum value, ϵ_u. Since a tensile strain of 0.01 is roughly two to five times the yield strain for typical anchor materials, both rows of anchors will have yielded.

This somewhat arbitrary limit ensures that the innermost row of tension anchors will approach their tensile strength prior to tensile failure of the outermost row of tension anchors. The limit has little effect on typical designs, since the flexural capacity of the connection is always maximized by locating the tension anchors as far as possible from the compressive reaction.

To properly assess the behavioral model, it was necessary to determine the assumed tension distribution which would give the highest predicted strength of the connection. This was accomplished by considering a connection with two rows of anchors in the tension zone and no anchors in the compression zone. Fig. 32 shows the connection used to determine the assumed tension distribution which produces the highest predicted strength.

The type of connection shown in Fig. 32 covers both areas of connection strength. If the load eccentricity, e, is greater than or equal to e', the strength of the connection is dominated by moment and is controlled by the tensile strength of the anchors in the tension zone. For this condition it is obvious that the maximum predicted strength occurs when both rows of anchors reach their tensile strength, T_0. If the load eccentricity, e, is less than e', the strength of the connection is dominated by shear and is controlled by shear strength of the anchors in the compression zone and by the combined tensile and shear strength of the anchors in the tension zone. For this condition it is not obvious which distribution of tension in the anchors produces the maximum predicted strength.

The distribution of tension which produces the maximum predicted strength in a shear-dominated connection was determined by the conditions of equilibrium. The moment equilibrium condition for the connection shown in Fig. 32 is given by:

$$V e = T_1 d_1 + T_2 d_2$$

$$V e = T_1 d_1 + \alpha T_1 ß d_1$$

$$V e = T_1 d_1 (1 + \alpha ß)$$

where: α = ratio of the tensile force in the inner row of anchors, T_2, to the tensile force in the outer row of anchors, T_1; $0 < \alpha \leq 1$

$ß$ = ratio of the distance between the inner row of anchors and the compressive reaction, d_2, to the distance between the outer row of anchors and the compressive reaction, d_1; $0.10 \leq ß \leq 1$

For a shear-dominated connection the tensile force in the outer row of anchors will be less than the tensile strength of the anchors, T_0:

$$V e = \delta T_0 d_1 (1 + \alpha ß)$$

where: δ = ratio of the tensile force in the outer row of anchors, T_1, to the tensile strength of a row of anchors, T_0; $0 < \delta \leq 1$

Rearranging terms yields the following:

$$e / d_1 = \delta (1 + \alpha ß) / (V / T_0) \quad (17)$$

The condition of normal force equilibrium for the connection shown in Fig. 32 is given by:

$$C = T_1 + T_2$$

$$C = T_1 (1 + \alpha) \quad (18)$$

The condition of shear force equilibrium for the connection shown in Fig. 32 is given by:

$$V = \mu C + V_1 + V_2 \quad (19)$$

Substituting Eq. (18) and Eq. (7) for elliptical tension/shear interaction into Eq. (19) gives:

$$V = \mu T_1 (1 + \alpha) + \gamma \sqrt{T_0^2 - T_1^2} + \gamma \sqrt{T_0^2 - \alpha T_1^2}$$

Substituting δT_0 for T_1 gives:

$$\frac{V}{T_0} = \mu \delta (1 + \alpha) + \gamma \sqrt{1 - \delta^2} + \gamma \sqrt{(1 - \delta^2 \alpha^2)} \quad (20)$$

Eq. (20), which represents the condition of force equilibrium for a connection with $e < e'$ and with anchors having an elliptical tension/shear interaction; and Eq. (17), which represents the condition of moment equilibrium for the same connection, are interdependent. These two equations were solved by assuming values of δ between zero and unity, which represents the range of application of Eq. (20), for various assumed values of α and ß. The value of (V/T_0) determined from Eq. (20) was used in Eq. (17) to find the corresponding value of (e/d_1). The results are shown in Fig. 33.

To show continuity between the area of behavior dominated by shear, $e < e'$, and the area of behavior dominated by moment, $e \geq e'$; Fig. 33 includes the area of behavior dominated by moment for the assumed values of α and ß. This area of behavior was determined from Eq. (17) with δ equal to unity, that is, $T_1 = T_0$, and taking $e \geq e'$:

$$V / T_0 = (1 + \alpha \beta) / (e / d_1) \qquad (21)$$

The maximum predicted strength of the connection in the area dominated by shear, ($e < e'$), and the area of behavior dominated by moment, ($e \geq e'$), occurs when the tensile force in the inner row of anchors is equal to the tensile force in the outer row of anchors ($\alpha = 1$). This is true for various locations of the inner row of anchors ($\beta = 0.25$, 0.50, and 0.75). Analogous derivations for the more conservative assumption of a linear tension/shear interaction of anchor strength are given in Ref. 4.

To summarize, the maximum predicted strength of a ductile connection with multiple rows of anchors in the tension zone can be determined by assuming equal tension in all the anchors in the tension zone. This is true for connections dominated by moment ($e \geq e''$), and connections dominated by shear ($e < e''$). The assumption of equal tension also implies equal shear in all the anchors in the tension zone for connections dominated by shear.

Analytically, the assumption of equal tension and shear in all the anchors in the tension zone is very convenient. The forces in all the anchors in the tension zone can be considered as a single force acting at the centroid, d, of the anchors in the tension zone.

Strength of connections dominated by moment--When the moment/shear ratio, e, of the applied loading is greater than or equal to the critical eccentricity, e", the strength of the connection is controlled by the tensile strength of the anchors in the tension zone.

The moment equilibrium condition for the typical connection of Fig. 34, with $e > e''$ ($T_n = T_0$), gives the strength of the connection as controlled by the tensile strength of the anchors in the tension zone:

$$V_{ut}\, e = n\, T_o\, d$$

$$V_{ut} = n\, T_o\, d / e \qquad (22)$$

where:

- V_{ut} = maximum predicted strength of the connection when the moment/shear ratio, e, of the applied loading is greater than or equal to the critical eccentricity, e", given by Eq. (8-10)
- n = number of rows of anchors in the tension zone
- T_o = tensile strength of a row of anchors in the tension zone

d = distance from the compressive reaction to the centroid of the tension anchors

Maximum predicted strength for connections dominated by shear ($e < e''$)--When the moment/shear ratio, e, of the applied loading is less than the critical eccentricity, e", the strength of the connection is controlled by the shear strength of the anchors in the compression zone, and by the combined tensile and shear strength of the anchors in the tension zone.

The condition of shear force equilibrium for the typical connection (shown in Fig. 34, with $e < e''$) is given by:

$$V_{ut} = \mu C + m V_o + n V_n \quad (23)$$

The condition of normal force equilibrium for that same connection with $e < e''$ is given by:

$$C = n T_n \quad (24)$$

Substituting Eq. (24) and Eq. (7) for elliptical tension/shear interaction into Eq. (23) yields the following:

$$V_{ut} = \mu n T_n + m\gamma T_o + n\gamma\sqrt{T_o^2 - T_n^2} \quad (25)$$

The condition of moment equilibrium for that same connection shown with $e < e''$ is given by:

$$V_{ut}\, e = n T_n d$$

$$T_n = V_{ut}\, e / (n d) \quad (26)$$

Substituting Eq. (26) into Eq. (25) and solving the resulting quadratic equation for V_{ut} gives:

$$V_{ut} = \gamma T_o \frac{ma + \sqrt{n^2(a^2 + b^2) - m^2 b^2}}{a^2 + b^2} \quad (27)$$

where: V_{ut} = maximum predicted strength of the connection when the moment/shear ratio, e, of the applied loading is less than the critical eccentricity, e", given by Eq. (16)

γ = ratio of the shear strength of the anchor to the tensile strength of the anchor

T_o = tensile strength of a row of anchors in the tension zone

m = number of rows of anchors in the compression zone

n = number of rows of anchors in the tension zone

a = $1 - \mu\ e / d$

b = $\gamma\ e / d$

μ = coefficient of friction between steel and concrete

d = distance from the compressive reaction to the centroid of the tension anchors

For the more conservative assumption of linear tension/shear interaction, the maximum predicted strength of the connection when e < e" is given by:

$$V_{ut} = \gamma\ T_o \frac{m + n}{1 + (\gamma - \mu)\left(\frac{e}{d}\right)} \qquad (28)$$

The maximum predicted strength of any ductile multiple-anchor connection is given by Eq. (22) for connections dominated by moment (e ≥ e"); and by Eq. (27) for connections dominated by shear (e < e"). The critical eccentricity, e", is defined by Eq. (16). Eq. (27) is based on an elliptical tension/shear interaction. The maximum predicted strength using the more conservative linear tension/shear interaction is given by Eq. (28).

Assessment of Behavioral Model

In this section, the results of the ultimate load tests are compared to the connection strengths predicted by the behavioral model.

The ratio between the shear strength and the tensile strength of the anchor, γ, used in calculating the predicted strengths is taken from Chapter 7 of Ref. 4 (γ = 0.50 for cast-in-place and adhesive anchors, γ = 0.60 for undercut anchors). For both graphical and tabular comparisons of this section the coefficient of friction, μ, used in calculating the predicted strengths, is the design value of 0.40 recommended earlier. The tabular comparisons

also include the predicted strengths calculated using a coefficient of friction, μ, of 0.50. As discussed previously, this value for the coefficient of friction represents an upper bound to the results of the friction tests. The compressive reaction is assumed to act at the toe of the baseplate for the rigid baseplate tests, and at the location recommended above for the flexible baseplate tests.

Two-anchor pattern--As indicated by Fig. 35 and Table 7, the predicted strengths calculated using an elliptical tension/shear interaction with the recommended values of μ and γ are in close agreement with the test results.

Four-anchor pattern--As indicated by Fig. 36 and Table 8, the predicted strengths calculated using an elliptical tension/shear interaction with the recommended values of γ and μ, agree closely with the test results. As shown by Table 8, the predicted strengths for the four-anchor pattern are not particularly sensitive to the assumed value of the coefficient of friction ($\mu = 0.40$ or $\mu = 0.50$).

Six-anchor pattern--As indicated by Fig. 37 and Table 9, the predicted strengths calculated using an elliptical tension/shear interaction with the recommended values of γ and μ, agree closely with the test results. As shown by Table 9, the predicted strengths for the six-anchor pattern are not particularly sensitive to the assumed value of the coefficient of friction ($\mu = 0.40$ or $\mu = 0.50$).

CONCLUSIONS

1) The coefficient of friction between a surface-mounted steel baseplate and hardened concrete in multiple-anchor connections, μ, should be taken as 0.40 with a strength reduction factor, ϕ, of 0.65. Based on the results of the 44 friction tests conducted in this study, the actual strength will then exceed the calculated design strength 98% of the time.

2) An elliptical tension/shear interaction relationship is appropriate for anchors in steel-to-concrete connections. A linear tension/shear interaction relationship is conservative.

3) The shear strength of cast-in-place and adhesive anchors in a multiple-anchor connection should be taken as 50% of the tensile strength ($V_o/T_o = \gamma = 0.50$). The shear strength of undercut anchors in a multiple-anchor connection should be taken as 60% of the tensile strength ($V_o/T_o = \gamma = 0.60$).

4) A design procedure based on limit design theory is appropriate for ductile multiple-anchor steel-to-concrete connections.

5) Ductile steel-to-concrete connections can be divided into two distinct areas of behavior depending on the moment-to-shear ratio of the applied loading:

   a) An area dominated by the applied moment. For connections in the moment-dominated area of behavior, the anchors in the tension zone can be assumed to attain their tensile strength prior to failure of the connection. In this case, the combined shear strength provided by the frictional force at the steel/concrete interface (due to the compressive reaction from the applied moment) and by the shear strength of anchors in the compression zone, exceeds the applied shear. The strength of these connections is controlled by the tensile strength of the anchors in the tension zone.

   b) An area dominated by the applied shear. For connections in the shear-dominated area of behavior, the anchors in the tension zone can be assumed to act as a single composite anchor acting at the centroid of the anchors in the tension zone. The strength of this composite anchor is limited by the anchors' tension/shear interaction relationship. In this case, anchors in the compression zone can be assumed to be at their maximum shear strength. The strength of these connections is controlled by the shear strength of the anchors in the compression zone, coupled with the combined tensile and shear strength of the anchors in the tension zone.

6) Baseplate flexibility affects the assumed location of the compressive reaction from the applied moment. To locate the compressive reaction from the applied moment in a conservative manner, the reaction can be considered to be located at a distance, x_{min}, determined by Eq. (5), from the outer edge of the compression element of the attached member. If the baseplate thickness is unknown, it is conservative to consider the compressive reaction to be located directly under the outer edge of the outermost compression element of the attached member.

7) The design recommendations resulting from this study are incorporated into a Design Guide for Steel-to-Concrete Connections (5). The Design Guide is the final report on Texas SDHPT Project 1126.

ACKNOWLEDGMENTS

The test results described here were obtained at the Phil M. Ferguson Structural Engineering Laboratory, Balcones Research Center, The University of Texas at Austin. Assistance of Laboratory technical and secretarial staff is gratefully acknowledged. The primary sponsor for the work was the Texas State Department of Highways and Public Transportation (Project 3-5-87-1126, "Design Guide for Short Anchor Bolts"). The Texas SDHPT contact was Mark McClelland. Supplemental sponsorship was also provided by the following anchor or adhesive manufacturers: Drillco; HILTI; ITW Ramset; Kelken-Gold, Inc.; SIKA Corporation; and Unifast Industries. These and other manufacturers were also generous with their products and technical expertise. Without the cooperation of many segments of the anchor industry, the research described here would not have been possible.

REFERENCES

1. ACI Committee 349, Code Requirements for Nuclear Safety Related Structures (ACI 349-85), American Concrete Institute, Detroit, 1985.

2. "All Projects, Steel to Concrete Coefficient of Friction, Preliminary Tests," TVA CEB Report No. 77-46, Tennessee Valley Authority, Knoxville, 1977.

3. Collins, D. M., Cook, R.A., Klingner, R. E. and Polyzois, D., "Load-Deflection Behavior of Cast-in-Place and Retrofit Concrete Anchors Subjected to Static, Fatigue, and Impact Tensile Loads," Research Report CTR 1126-1, Center for Transportation Research, The University of Texas at Austin, February 1989.

4. Cook, R. A. and Klingner, R. E., "Behavior and Design of Multiple-Anchor Baseplate Connections," Research Report CTR 1126-3, Center for Transportation Research, The University of Texas at Austin, March 1989.

5. Cook, R. A., Doerr, G. T., Collins, D. M. and Klingner, R. E., "Design Guide for Steel-to-Concrete Connections," Report No. 1126-4F, Center for Transportation Research, University of Texas at Austin, March 1989.

6. Doerr, G. T., Cook, R. A. and Klingner, R. E., "Adhesive Anchors: Load-Deflection Behavior and Spacing Requirements," Research Report CTR 1126-2, Center for Transportation Research, The University of Texas at Austin, March 1989.

7. "Eight-Bolt Base Plate Tests," Report No. EQL 65/84 E, Hilti Technical Center, 1984.

8. "General Anchorage to Concrete," TVA Civil Design Standard No. DS-C1.7.1, Tennessee Valley Authority, Knoxville, TN, 1984.

9. Manual of Steel Construction, Load and Resistance Factor Design, 1st Edition, American Institute of Steel Construction, Chicago, Ill., 1986.

10. PCI Design Handbook - Precast and Prestressed Concrete, 3rd Edition, Prestressed Concrete Institute, Chicago, 1985.

TABLE 1 -- SUMMARY OF PROCEDURES FOR CALCULATING DESIGN TENSILE STRENGTH OF STEEL

Reference	Type of Anchor	Nominal Strength[1,2] T_n	Strength Reduction Factor ϕ
PCI[3] (10)	Stud	$0.9\ A_s\ F_y$	1.00
ACI (1)	Threaded or Stud	$A_s\ F_y$	0.90
TVA (8)	Threaded or Stud	$A_s\ F_y$	0.90
AISC[4] (9)	Threaded	$A_s\ F_u$	0.75

Notes: 1. The nominal tensile strength given in this table is based on the effective stress area of the anchor. For welded studs this is the gross area of the stud. For threaded anchors this is the tensile stress area as given in ANSI B1.1.

2. F_y is the minimum specified yield strength of the anchor steel. F_u is the minimum specified tensile strength of the anchor steel.

3. The 1985 PCI Design Handbook is only valid for welded studs. For threaded anchors the 1985 PCI Design Handbook references the AISC Specification.

4. The AISC Specification uses 75% of the gross area of the anchor for the effective stress area of threaded anchors. This area is the same as the tensile stress area as given in ANSI B1.1 and used in this table.

TABLE 2 -- TEST MATRIX

TYPE OF TEST	e in.	TYPE OF ANCHOR (See Notes)								No. Tests
		CIP	M1	A1	A2	A3	A4	A5	A6	
Two-Anchor Rigid Baseplate	6	1	1	1	-	-	-	-	-	3
	12	1	1	1	-	-	1	-	-	4
	18	1	1	1	-	-	-	-	-	3
	24	1	1	-	-	-	1	-	-	3
	30	1	1	-	-	-	-	-	-	2
	36	1	1	-	-	-	1	-	-	3
										18
Four-Anchor Rigid Baseplate	6	1	1	1	-	-	1	-	-	4
	12	1	1	1	-	-	1	-	-	4
	18	1	1	1	-	-	1	-	-	4
	24	1	-	-	-	-	-	-	-	1
										13
Six-Anchor Rigid Baseplate	6	1	1	-	-	-	-	-	-	2
	12	1	1	1	1	1	1	1	1	8
	18	1	1	-	-	-	-	-	-	2
										12
Six-Anchor Flexible Baseplate	12	-	1	1	-	-	1	-	-	3
No. Tests		13	13	8	1	1	8	1	1	46

NOTES:

CIP = cast-in-place anchors
M1 = undercut anchor by Drillco (MAXIBOLT)
A1 = adhesive anchor by Ramset (EPCON)
A2 = adhesive anchor by Hilti (HIT)
A3 = adhesive anchor by Hilti (HVA)
A4 = adhesive anchor by Kelken (KELI-GROUT)
A5 = adhesive anchor by Sika (SIKA GEL)
A6 = adhesive anchor by Sika (SIKA INJECTION)

TABLE 3 -- CONCRETE CYLINDER STRENGTHS

Pour No.	Compressive Strength at 28 days (psi)	Compressive Strength at Testing (psi)
1	4500	5750-6500
2	5000	5500-6500
3	4000	4500-6500
4	6000	6000-6500
5	5500	6500-6750
6	6000	6250-6750
7	4500	4750
8	4500	4500
9	4500	5500

TABLE 4 -- ANCHOR TENSILE STRENGTH FROM UNIVERSAL TESTING MACHINE

	TYPE OF ANCHOR or TENSILE STRENGTH (kips)		
	Cast-In-Place	Undercut	Adhesive
	32.3 31.1	32.5 31.9 31.3	31.4 31.0 29.7 31.1 29.6
Mean	31.7	31.9	30.6

Note: Mean for all ten tests = 31.2 kips

Standard deviation = 3%

TABLE 5 -- SUMMARY OF FRICTION TEST RESULTS

SUMMARY OF FRICTION TESTS							
	Test Variables				Coefficient of Friction, μ		
Test No.	Seq. Test No.	Test Block Surf.	Comp. Force kips	Type of Test 1	max	min	mean
2 CIP 6	8	Top	18	All	.50	.46	.48
2 A1 6	24	Btm	18	All	.39	.35	.38
2 M1 6	28	Btm	28	All	.42	.34	.36
2 CIP 12	3	Top	18	All	.41	.35	.38
2 A1 12	25	Btm	16	All	.38	.35	.36
2 A4 12	26	Btm	16	All	.49	.37	.43
2 M1 12	27	Btm	25	All	.37	.30	.32
2 CIP 18	14	Top	11	All	.43	.38	.39
2 A1 18	12	Btm	9	All	.38	.37	.38
2 M1 18	37	Btm	39	Toe *	.42	.42	.42
2 CIP 24	1	Top	16	All	.39	.36	.38
2 A4 24	29	Btm	16	All	.55	.43	.50
	30	Btm	31	Toe *	.43	.43	.43
2 M1 24	38	Btm	36	Toe *	.48	.48	.48
2 CIP 30	2	Top	17	All	.48	.43	.47
2 M1 30		Btm		6 M1 18			
2 CIP 36	4	Top	18	All	.39	.34	.37
2 A4 36	23	Top	18	All	.22	.20	.21
2 M1 36		Btm		4 M1 18			
4 CIP 6	9	Top	20	All	.48	.44	.46
	10	Top	15	Toe *	.41	.41	.41
4 A1 6	7	Top	23	All	.41	.34	.37
4 A4 6	32	Top	20	Toe	.57	.47	.53
4 M1 6	31	Btm	28	Toe	.37	.34	.35
4 CIP 12	15	Top	29	All	.44	.39	.41
4 A1 12	6	Top	31	All	.40	.34	.37
4 A4 12	20	Top	20	All	.51	.46	.47
4 M1 12	33	Btm	40	Toe	.63	.53	.58
4 CIP 18	13	Top	29	All	.36	.32	.34
4 A1 18	11	Btm	22	All	.58	.50	.54
4 A4 18	21	Top	26	All	.36	.30	.32
4 M1 18	34	Btm	34	Toe	.62	.51	.57
4 CIP 24	5	Top	24	All	.61	.51	.56
6 CIP 6	36	Top	40	All	.32	.26	.27
6 M1 6	41	Btm	27	Toe	.61	.53	.57
6 CIP 12	17	Top	22	All	.51	.47	.50
6 A1 12	35	Top	40	All	.33	.28	.31
6 A2 12		Top		No Test			
6 A3 12		Top		No Test			
6 A4 12	22	Top	30	All	.62	.53	.58
6 A5 12	19	Btm	15	All	.37	.36	.36
6 A6 12	18	Btm	16	All	.52	.46	.49
6 M1 12	40	Btm	40	Toe	.60	.54	.58
6 CIP 18	16	Top	20	All	.47	.41	.44
6 M1 18	39	Btm	29	Toe	.51	.45	.47
6 A1 12X		Top	18	All	.50	.42	.48
6 A4 12X		Btm	16	All	.38	.26	.33
6 M1 12X		Top	40	All	.32	.28	.30
Total Number of Friction Tests = 44				Average	.46	.39	.43
				Std. Dev.	.10	.09	.09

Note: "All" represents tests with all the corner anchors preloaded, "Toe" represents tests with only the anchors on the leading edge preloaded, "Toe " represents tests at high eccentricities without preload, and a reference to another test means that both tests were conducted on the same surface of the same block.

TABLE 6 -- MAXIMUM RECORDED APPLIED LOAD, ULTIMATED LOAD TESTS, FROM SEPARATE DATA ACQUISITION SYSTEMS

Test No.	Maximum Recorded Applied Load, V (kips)		
	HP Plotter	HP DAS	Difference
2 M1 6	49.1	49.0	0.1
2 CIP 12	41.1	40.8	0.3
2 A1 12	52.2	52.2	0.0
2 M1 12	55.5	55.4	0.1
2 A1 18	47.1	46.2	0.9
2 M1 18	53.9	53.6	0.3
2 M1 24	44.9	44.6	0.3
2 A4 36	29.2	29.2	0.0
2 M1 36	31.1	31.1	0.0
4 CIP 6	74.4	70.0	4.4
4 A4 6	81.8	81.3	0.5
4 M1 6	86.9	86.6	0.3
4 A4 12	77.1	76.6	0.5
4 M1 12	85.9	85.7	0.2
4 CIP 18	58.3	57.9	0.4
4 A4 18	58.3	58.1	0.2
4 M1 18	63.9	63.3	0.6
6 CIP 6	107.8	107.2	0.6
6 M1 6	137.0	136.3	0.7
6 CIP 12	123.6	123.5	0.1
6 A1 12	110.6	109.6	1.0
6 A2 12	118.6	116.3	2.3
6 A3 12	125.3	124.5	0.8
6 A4 12	120.7	119.7	1.0
6 A5 12	104.7	104.5	0.2
6 A6 12	113.8	113.7	0.1
6 M1 12	130.5	129.8	0.7
6 CIP 18	86.8	86.4	0.4
6 A1 12X	107.7	105.5	2.2
6 A4 12X	104.8	103.8	1.0
6 M1 12X	110.4	109.7	0.7

TABLE 7 -- TEST RESULTS VERSUS PREDICTED STRENGTHS FOR TWO-ANCHOR SPECIMENS

Test No.	Vtest kips	μ = 0.40		μ = 0.50	
		Vut kips	Vtest / Vut	Vut kips	Vtest / Vut
2 CIP 6	37.0	35.4	1.05	36.8	1.01
2 A1 6	40.3	35.4	1.14	36.8	1.10
2 M1 6	49.1	42.1	1.17	43.7	1.12
2 CIP 12	41.1	38.8	1.05	42.1	0.98
2 A1 12	52.2	38.8	1.34	42.1	1.24
2 A4 12	46.5	38.8	1.20	42.1	1.10
2 M1 12	55.5	44.6	1.24	48.1	1.15
2 CIP 18	51.2	39.6	1.29	43.8	1.17
2 A1 18	47.1	39.6	1.16	43.8	1.07
2 M1 18	53.9	43.4	1.24	47.1	1.14
2 CIP 24	35.0	37.4	0.94	40.5	0.86
2 A4 24	44.6	37.4	1.19	40.5	1.10
2 M1 24	44.9	39.1	1.15	41.5	1.08
2 CIP 30	36.0	33.3	1.08	34.8	1.03
2 M1 30	38.4	33.9	1.13	34.9	1.10
2 CIP 36	29.6	29.0	1.02	29.3	1.01
2 A4 36	29.2	29.0	1.01	29.3	1.00
2 M1 36	31.1	29.1	1.07	29.3	1.06

TABLE 8 -- TEST RESULTS VERSUS PREDICTED STRENGTHS FOR FOUR-ANCHOR SPECIMENS

Test No.	V test kips	μ = 0.40		μ = 0.50	
		V ut kips	$\frac{V\ test}{V\ ut}$	V ut kips	$\frac{V\ test}{V\ ut}$
4 CIP 6	74.4	69.3	1.07	72.0	1.03
4 A1 6	75.2	69.3	1.08	72.0	1.04
4 A4 6	81.8	69.3	1.18	72.0	1.14
4 M1 6	86.9	81.7	1.06	84.7	1.03
4 CIP 12	76.7	69.6	1.10	73.8	1.04
4 A1 12	80.5	69.6	1.16	73.8	1.09
4 A4 12	77.1	69.6	1.11	73.8	1.04
4 M1 12	85.9	76.9	1.12	80.5	1.07
4 CIP 18	58.3	58.3	1.00	58.6	0.99
4 A1 18	59.9	58.3	1.03	58.6	1.02
4 A4 18	58.3	58.3	1.00	58.6	0.99
4 M1 18	63.9	58.6	1.09	58.6	1.09
4 CIP 24	40.5	43.9	0.92	43.9	0.92

TABLE 9 -- TEST RESULTS VERSUS PREDICTED STRENGTHS FOR SIX-ANCHOR SPECIMENS

Test No.	V test kips	μ = 0.40		μ = 0.50	
		V ut kips	V test / V ut	V ut kips	V test / V ut
6 CIP 6	107.8	107.7	1.00	113.3	0.95
6 M1 6	137.0	126.2	1.09	132.5	1.03
6 CIP 12	123.6	107.8	1.15	115.9	1.07
6 A1 12	110.6	107.8	1.03	115.9	0.95
6 A2 12	118.6	107.8	1.10	115.9	1.02
6 A3 12	125.3	107.8	1.16	115.9	1.08
6 A4 12	120.7	107.8	1.12	115.9	1.04
6 A5 12	104.7	107.8	0.97	115.9	0.90
6 A6 12	113.8	107.8	1.06	115.9	0.98
6 M1 12	130.5	117.0	1.12	123.5	1.06
6 CIP 18	86.8	88.7	0.98	89.6	0.97
6 M1 18	94.0	89.5	1.05	89.6	1.05
6 A1 12x	107.7	100.8	1.07	106.1	1.02
6 A4 12x	104.8	100.8	1.04	106.1	0.99
6 M1 12x	110.4	105.2	1.05	108.4	1.02

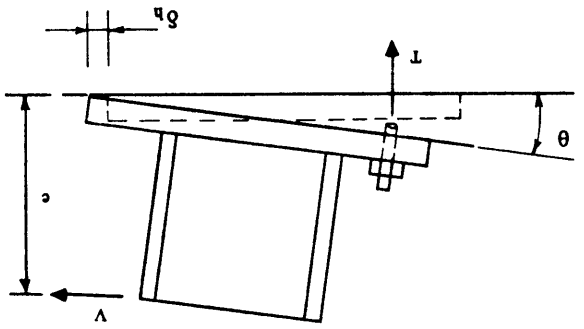

Fig. 1--Typical loading condition and measured values, test setup

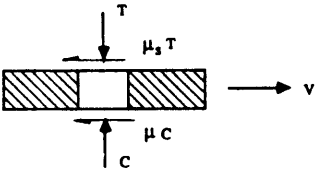

a) Free body diagram of baseplate

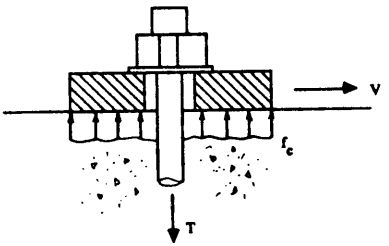

b) Free body diagram of baseplate with anchor

Fig. 2--Frictional forces on baseplate prior to anchor bearing

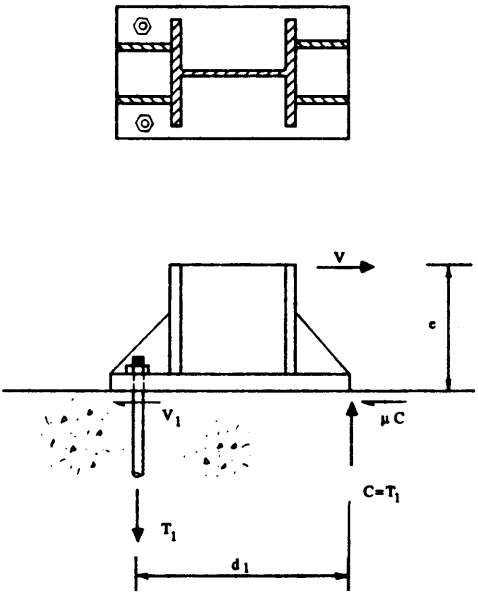

Fig. 3--Free body diagram of two-anchor rigid baseplate specimen

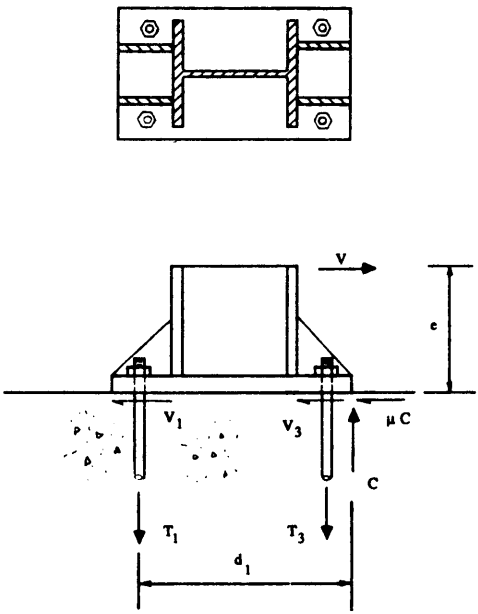

Fig. 4--Free body diagram of four-anchor rigid baseplate specimen

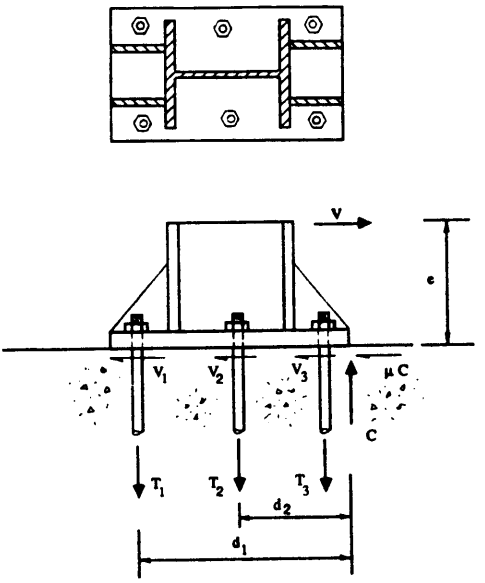

Fig. 5--Free body diagram of six-anchor rigid baseplate specimen

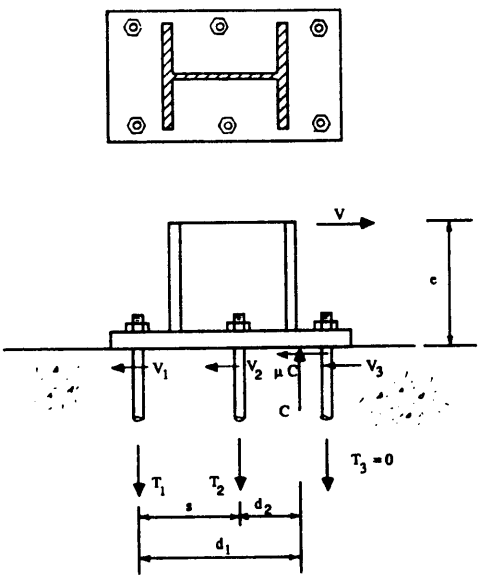

Fig. 6--Free body diagram of six-anchor flexible baseplate specimen

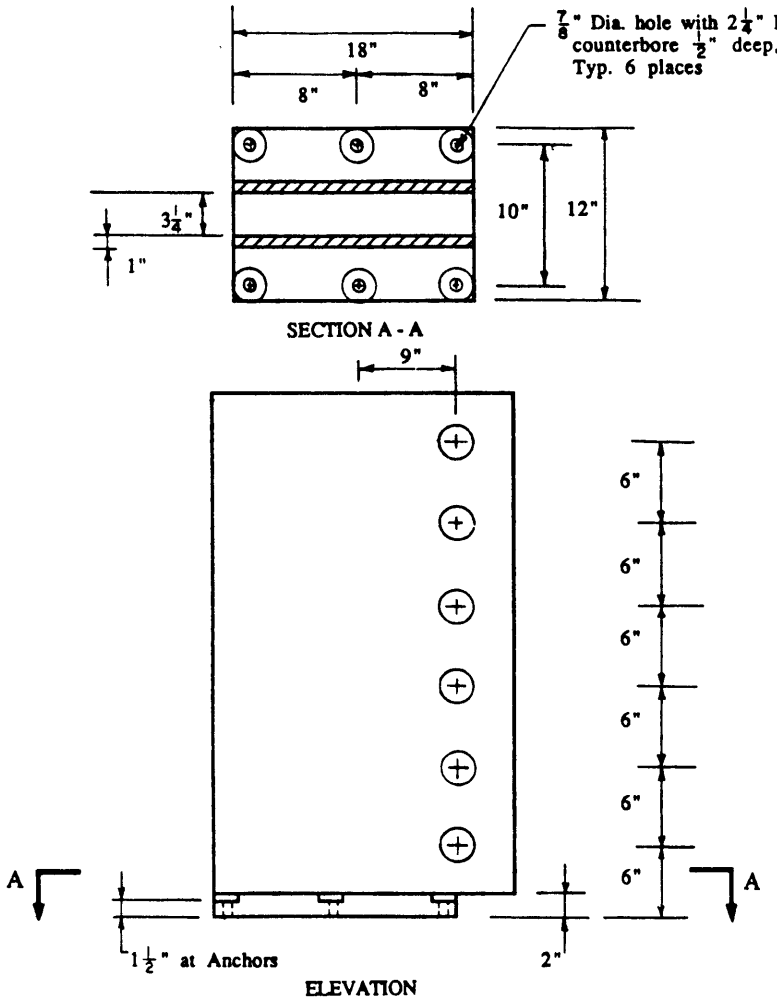

Fig. 7--Steel attachment for rigid baseplate tests

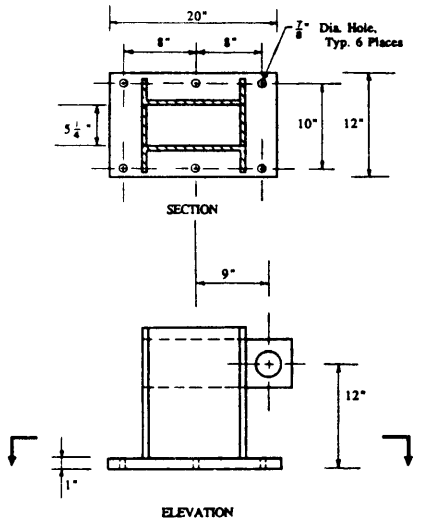

Fig. 8--Steel attachment for flexible baseplate tests

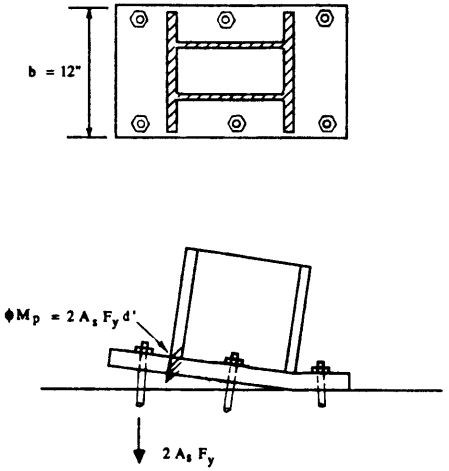

Fig. 9--Design basis for flexible baseplate tests

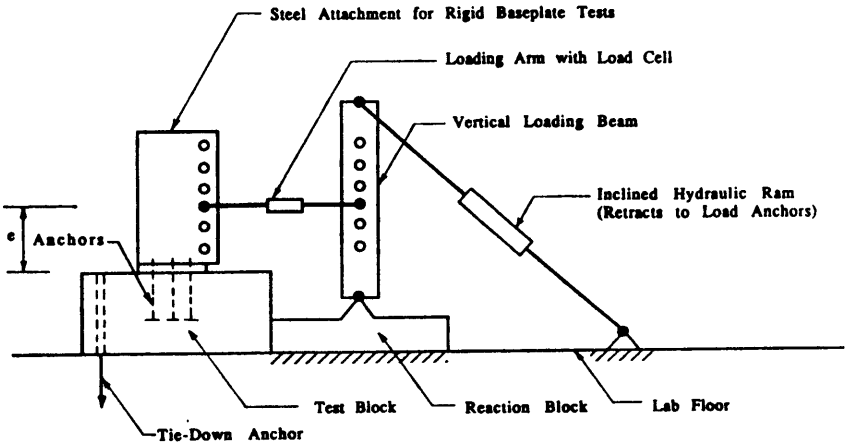

Fig. 10--Schematic diagram of test setup

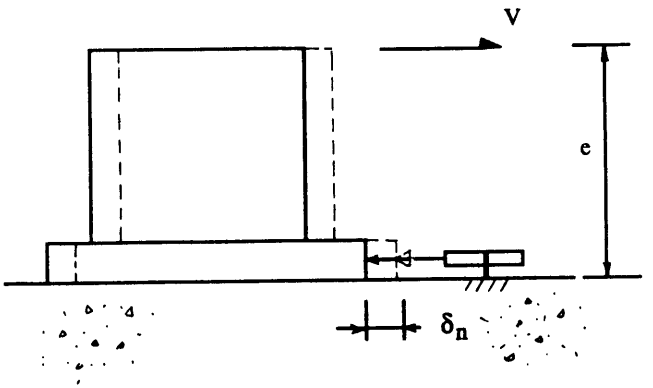

Fig. 11--Schematic diagram of slip measurement

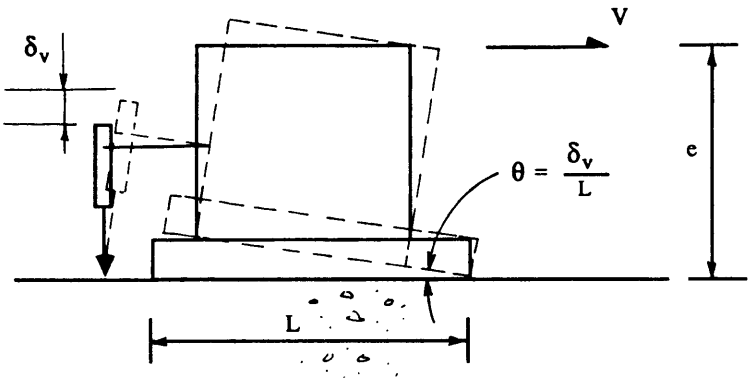

Fig. 12--Schematic diagram of rotation measurement for rigid baseplate tests

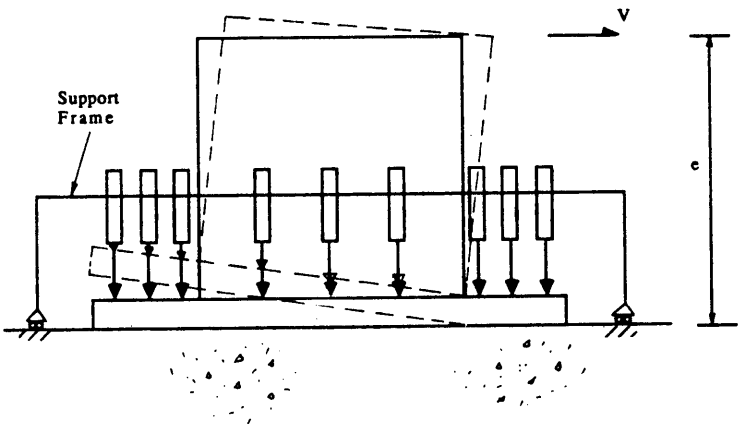

Fig. 13--Schematic diagram of vertical displacement measurement for flexible baseplate tests

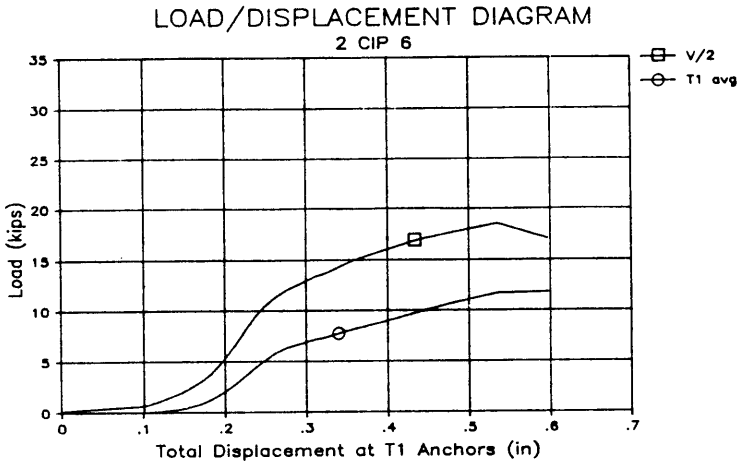

Fig. 14--Typical load-displacement diagram for two-anchor rigid baseplate test dominated by anchor shear

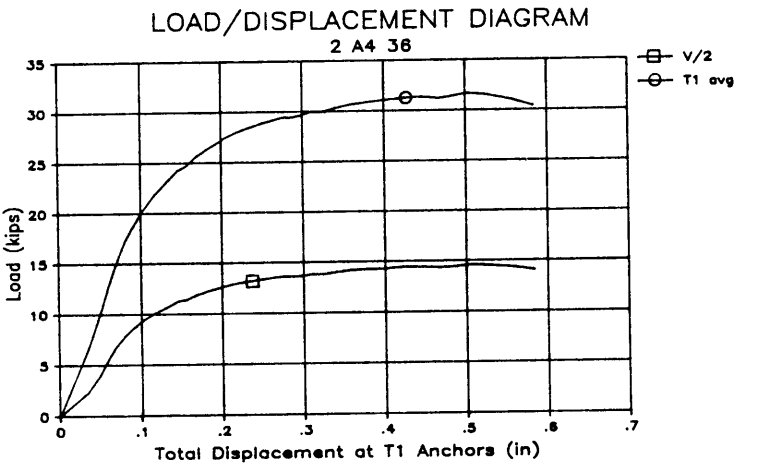

Fig. 15--Typical load-displacement diagram for two-anchor rigid baseplate test dominated by anchor tension

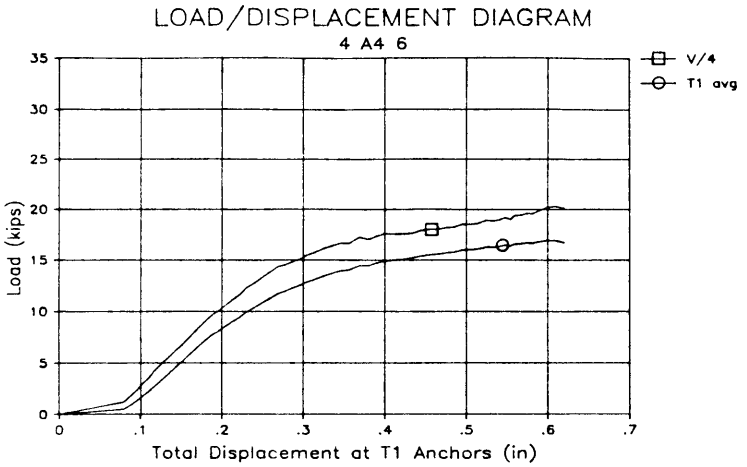

Fig. 16--Typical load-displacement diagram for four-anchor rigid baseplate test dominated by anchor shear

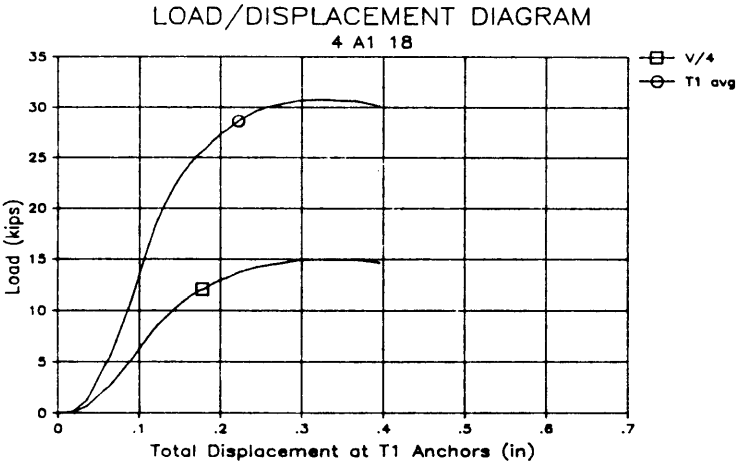

Fig. 17--Typical load-displacement diagram for four-anchor rigid baseplate test dominated by anchor tension

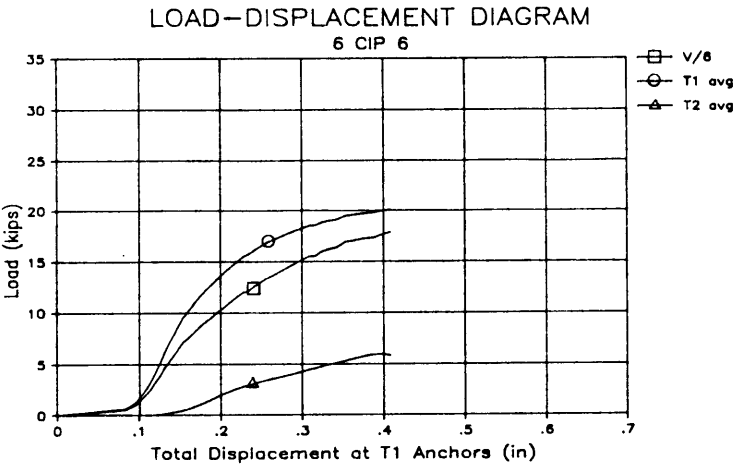

Fig. 18--Typical load-displacement diagram for six anchor rigid baseplate test dominated by anchor shear

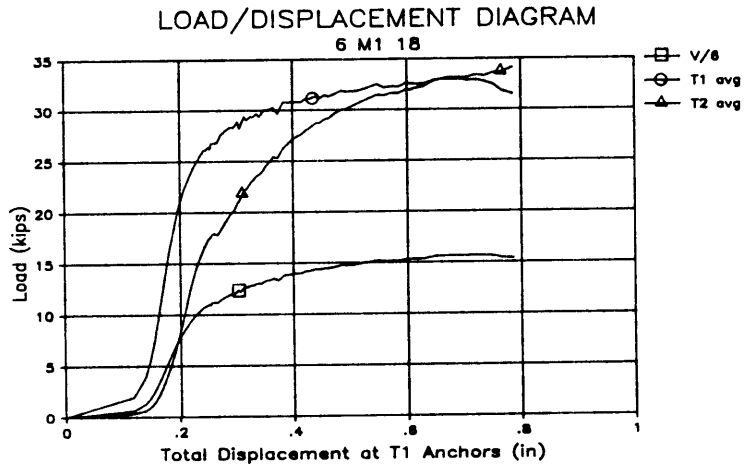

Fig. 19--Typical load-displacement diagram for six-anchor rigid baseplate test dominated by anchor tension

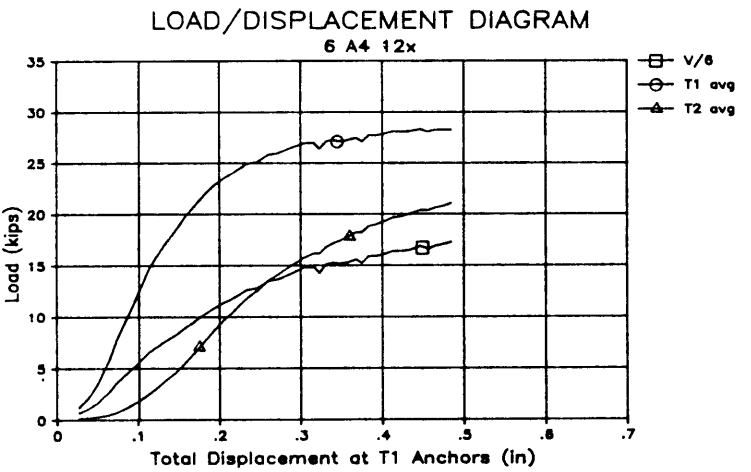

Fig. 20--Typical load-displacement diagram for six-anchor flexible baseplate test

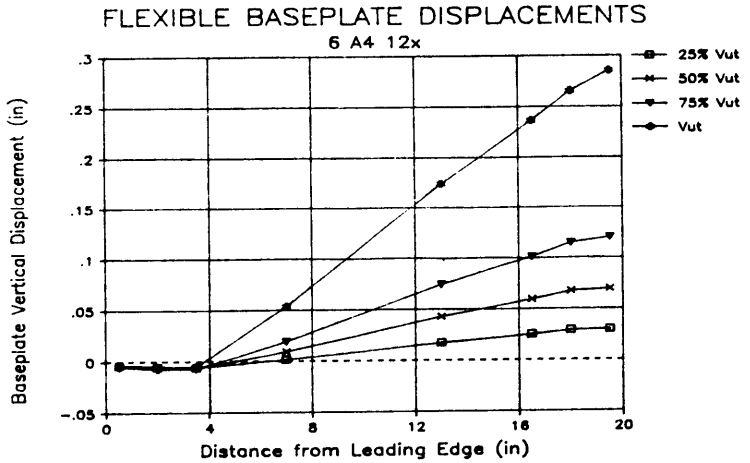

Fig. 21--Typical vertical displacements along the centerline of a flexible baseplate

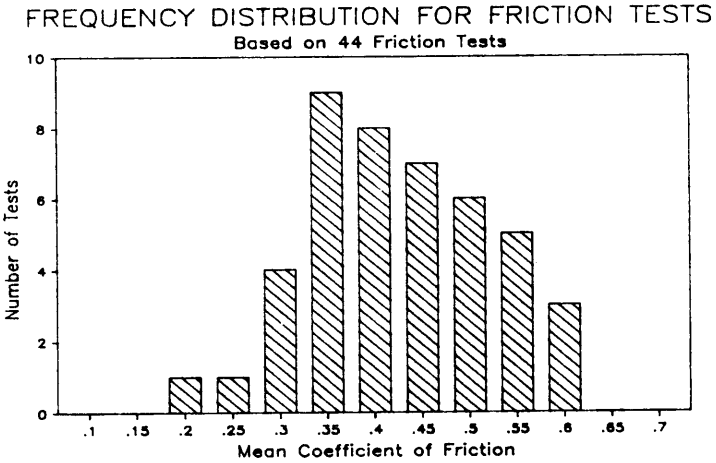

Fig. 22--Frequency distribution for friction tests

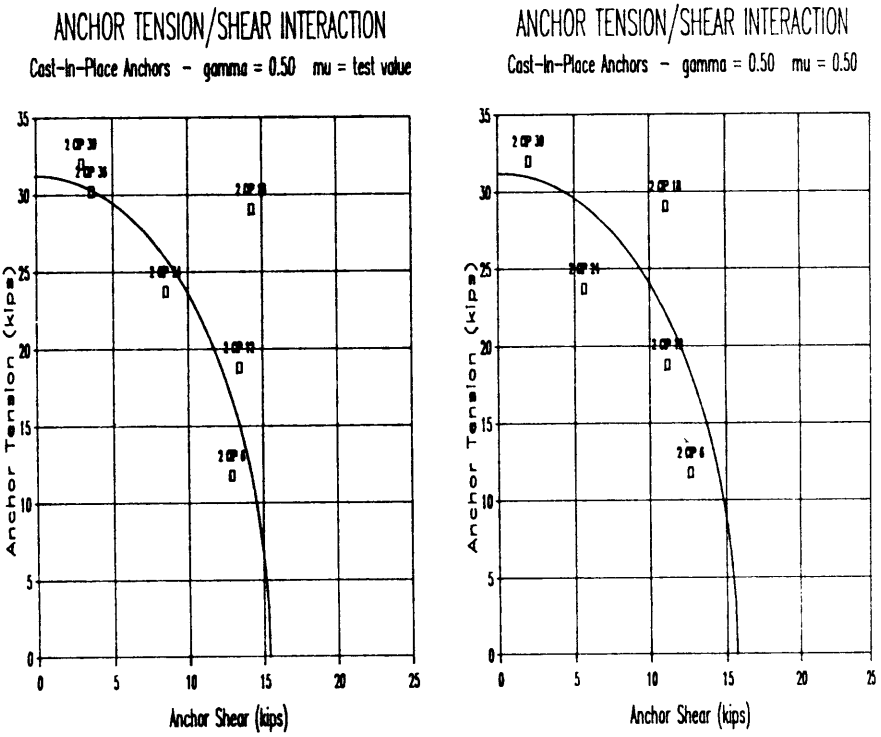

Fig. 23--Tension/shear interaction for cast-in-place anchors

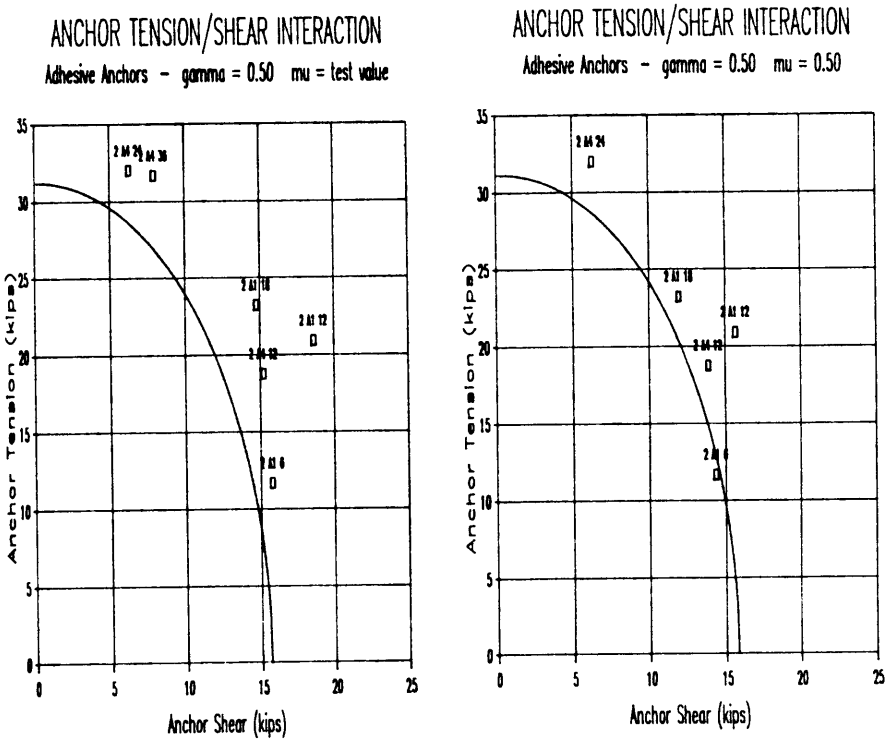

Fig. 24--Tension/shear interaction for adhesive anchors

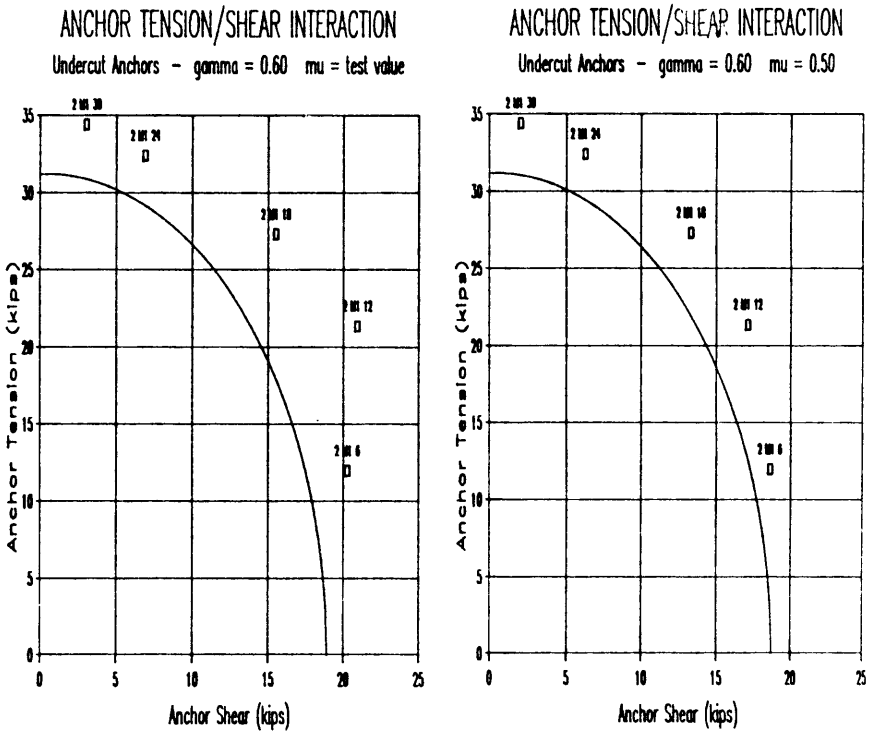

Fig. 25--Tension/shear interaction for undercut anchors

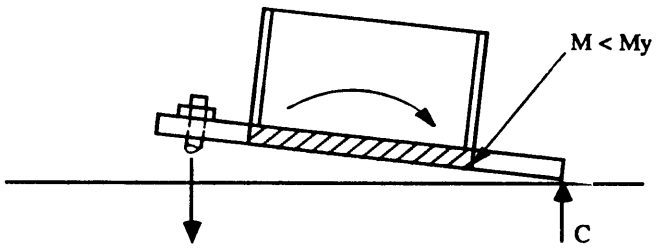

(a) Compressive Reaction at Toe

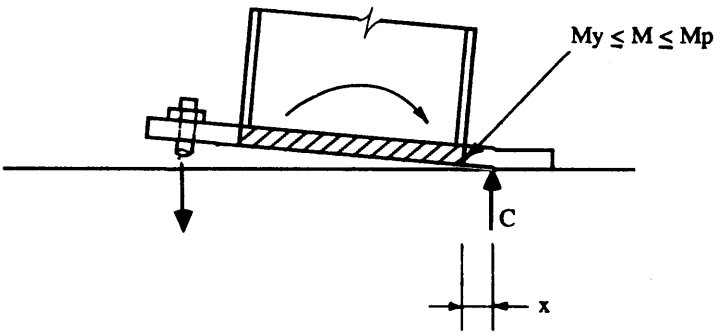

(b) Compressive Reaction Shifted in from Toe

Fig. 26--Effect of baseplate flexibility on location of compressive reaction

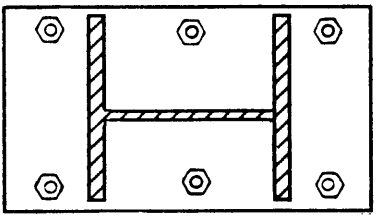

(a) PLAN VIEW

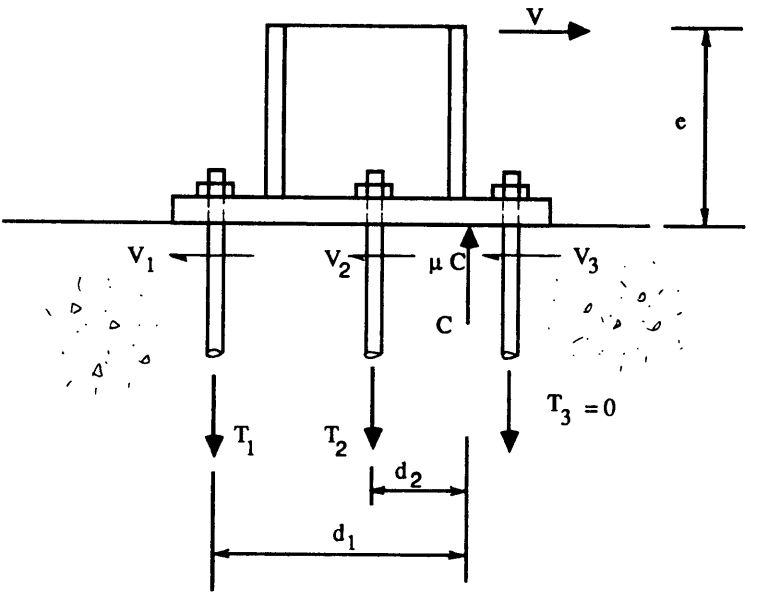

(b) SECTIONAL FREE BODY

Fig. 27--Possible distribution of forces on multiple-anchor connection

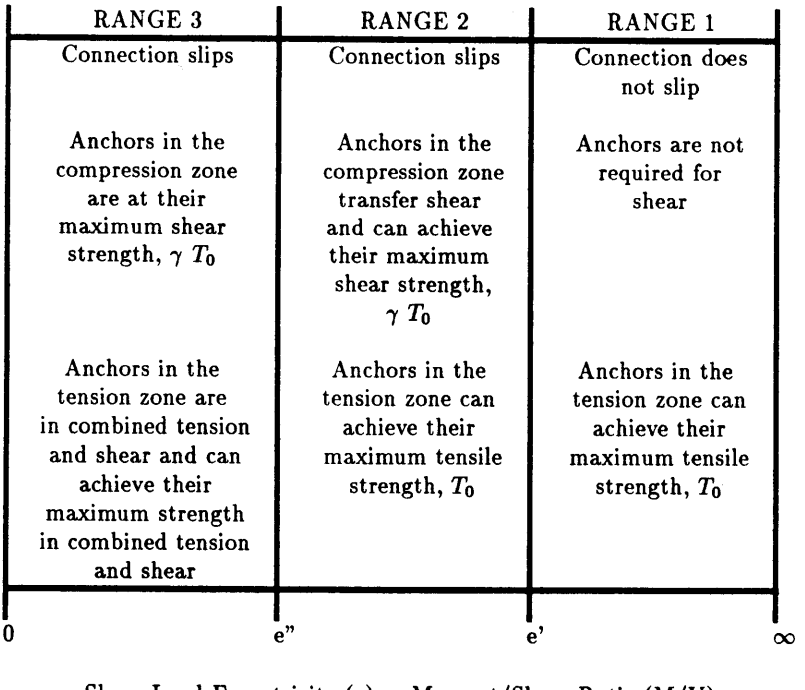

Fig. 28--Ranges of behavior for ductile multiple-anchor connection

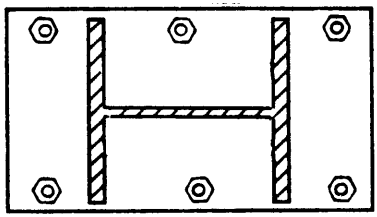

(a) PLAN VIEW

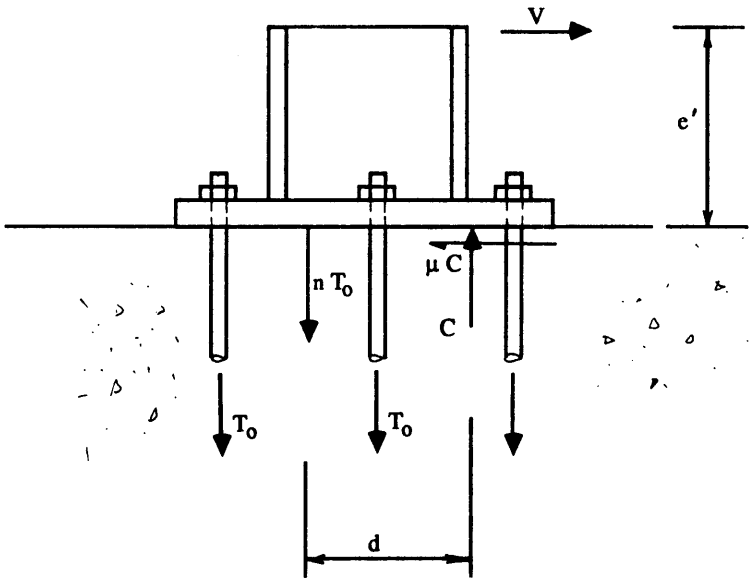

(b) SECTIONAL FREE BODY

Fig. 29--Forces on multiple-anchor connection with shear load eccentricity e'

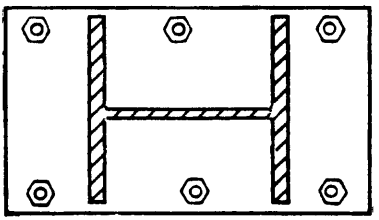

(a) PLAN VIEW

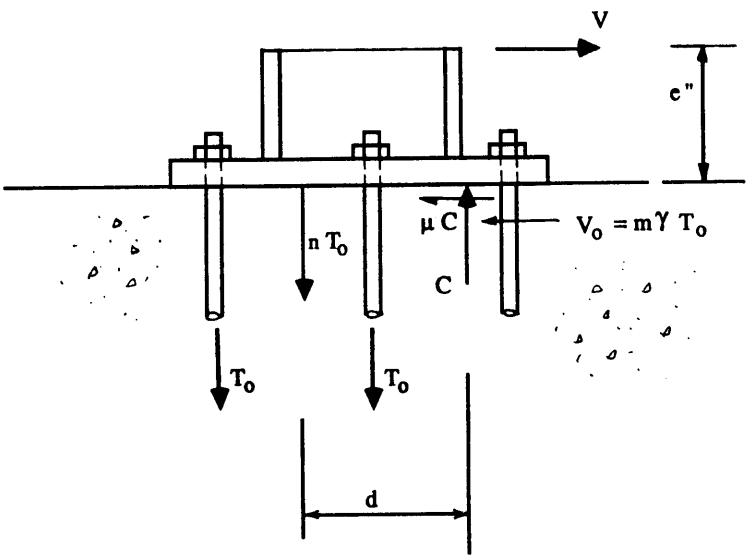

(b) SECTIONAL FREE BODY

Fig. 30--Forces on multiple-anchor connection with shear load eccentricity e"

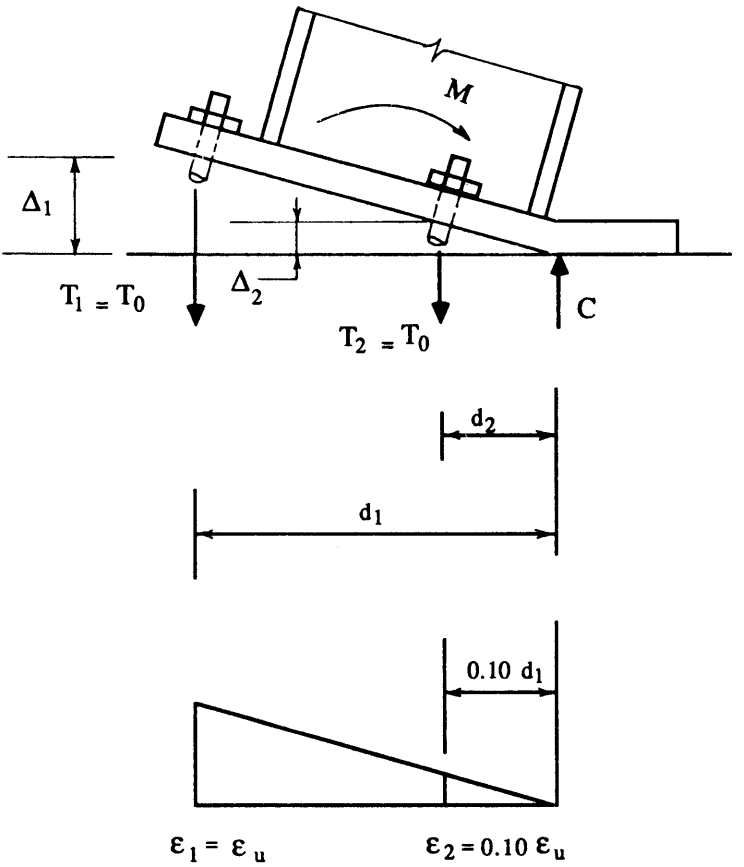

Tensile Strains at Ultimate Moment

Fig. 31--Limiting locations for tension anchors

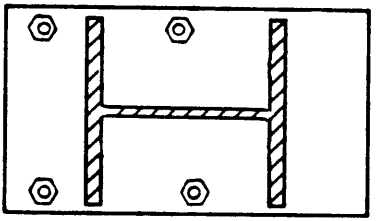

(a) PLAN VIEW

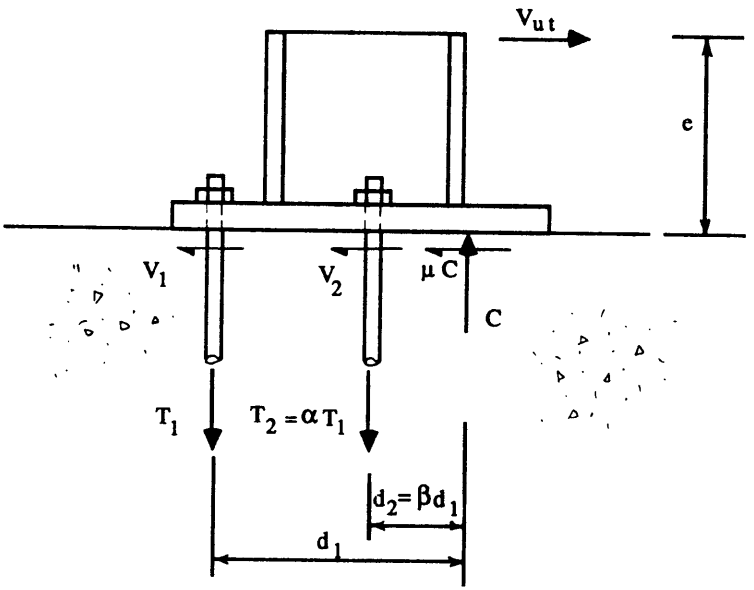

(b) SECTIONAL FREE BODY

Fig. 32--Example of connection used to assess maximum predicted strength

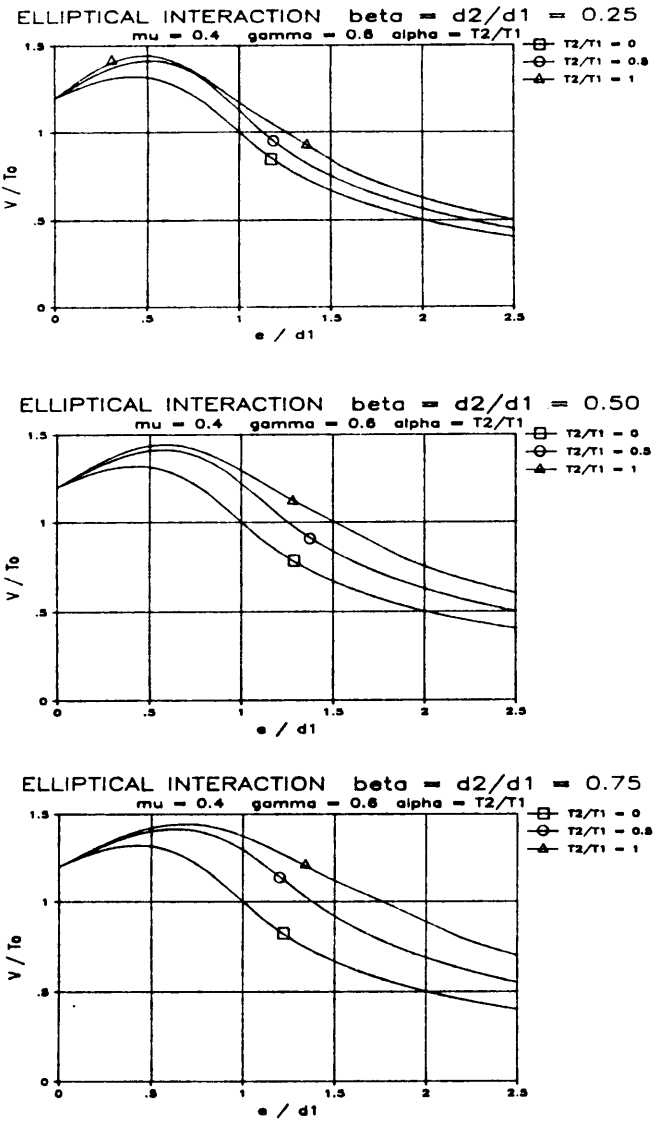

Fig. 33--Comparison of predicted strengths with elliptical tension/shear interaction

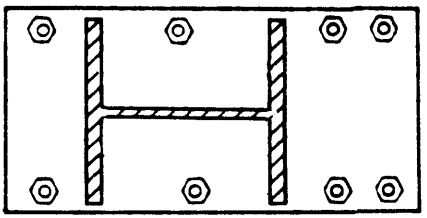

(a) PLAN VIEW

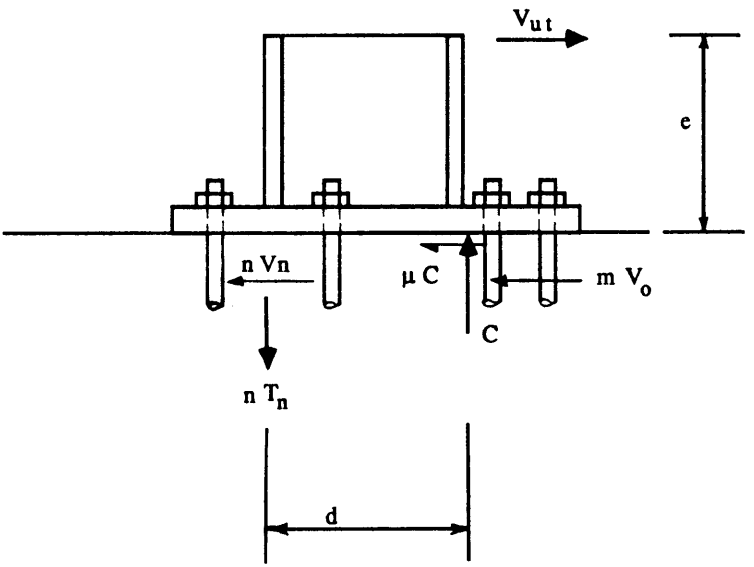

(b) SECTIONAL FREE BODY

Fig. 34--Possible distribution of forces on multiple-anchor connection for maximum predicted strength

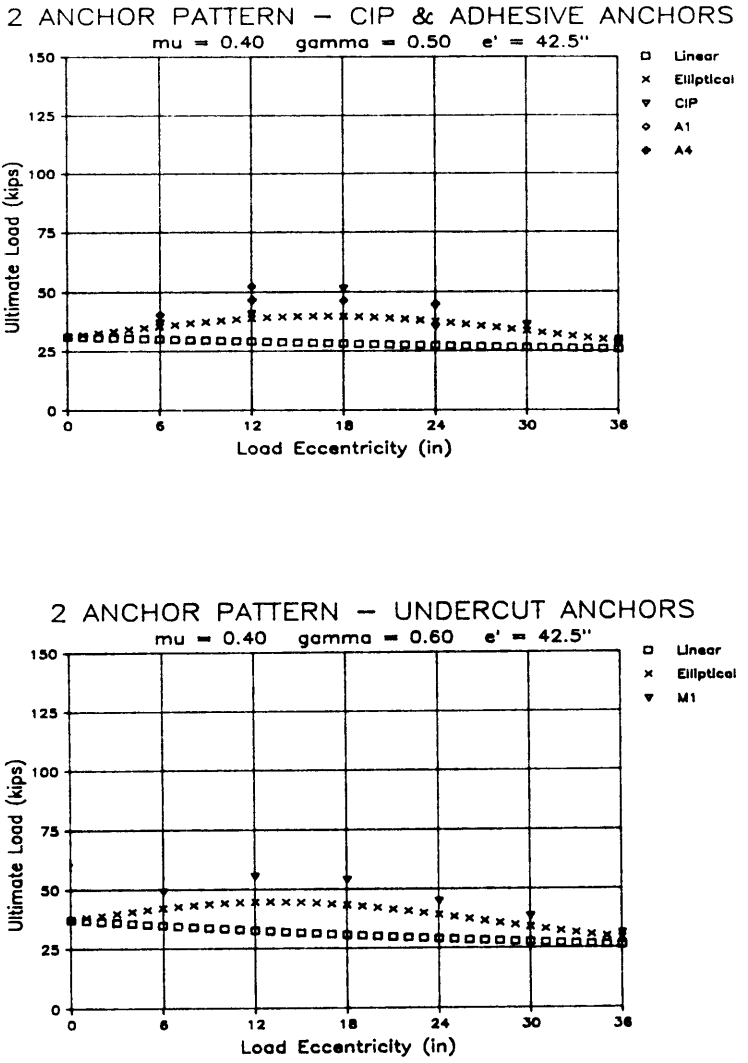

Fig. 35--Test results versus predicted strengths for two-anchor rigid baseplate specimens

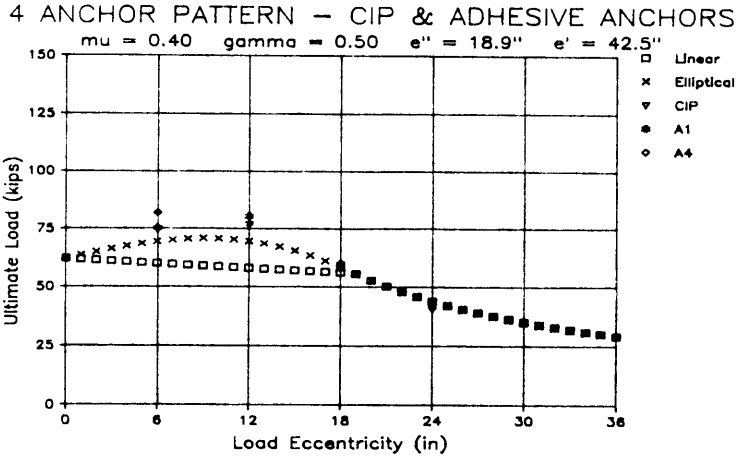

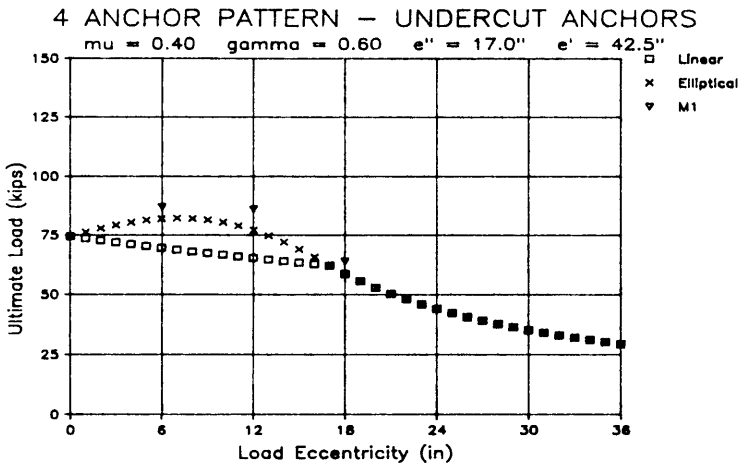

Fig. 36--Test results versus predicted strengths for four-anchor rigid baseplate specimens

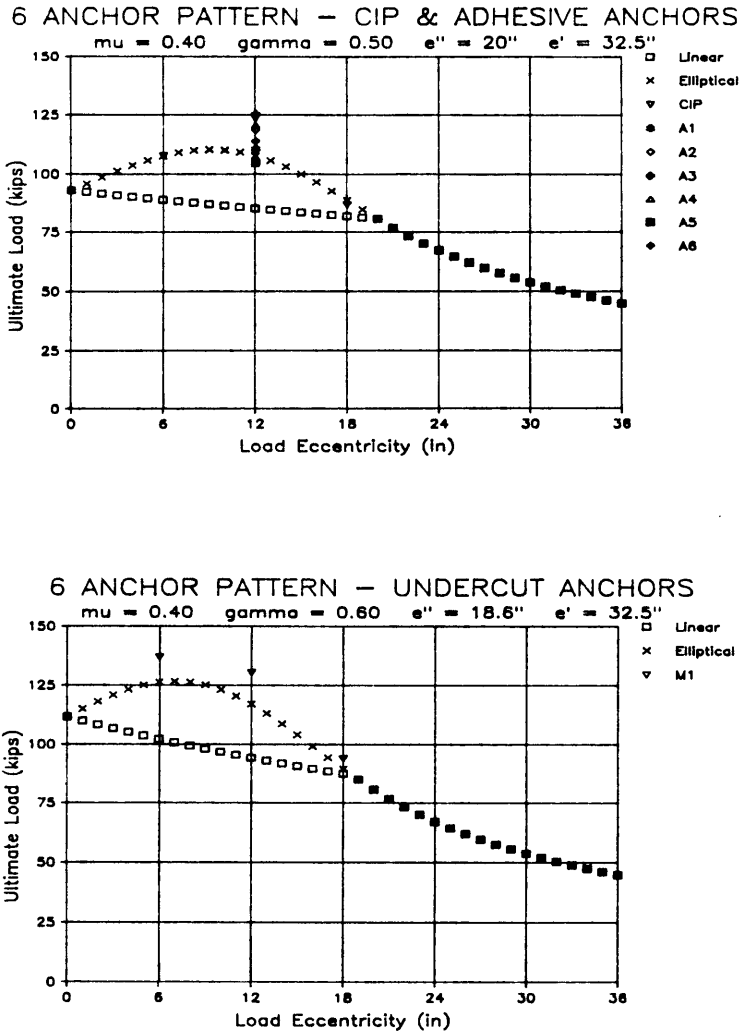

Fig. 37--Test results versus predicted strengths for six-anchor rigid baseplate specimens